

COLD DARK MATTER IN NON-STANDARD COSMOLOGIES, PAMELA, ATIC AND FERMI LAT

C. PALLIS

*Department of Physics, University of Patras,
GR-265 00 Patras, GREECE*

e-mail address: kpallis@auth.gr

ABSTRACT: We consider two non-standard cosmological scenaria according to which the universe is reheated to a low reheating temperature after the late decay of a scalar field or is dominated by the kinetic energy of a quintessence field in the context of a tracking quintessential model. In both cases, we calculate the relic density of the *Weakly Interacting Massive Particles* (WIMPs) and show that it can be enhanced with respect to its value in the standard cosmology. By adjusting the parameters of the low reheating or the quintessential scenario, the cold dark matter abundance in the universe can become compatible with large values for the annihilation cross section times the velocity of the WIMPs. Using these values and assuming that the WIMPs annihilate predominantly to e^+e^- or $\mu^+\mu^-$, we calculate the induced fluxes of e^\pm cosmic rays and fit the current data of PAMELA and ATIC or Fermi LAT. We achieve rather good fits especially to PAMELA and Fermi-LAT data in conjunction with a marginal fulfillment of other restrictions, arisen from nucleosynthesis and cosmic microwave background, provided that the WIMPs annihilate predominantly to $\mu^+\mu^-$. In both non-standard scenaria the required transition temperature to the conventional radiation dominated era turns out to be lower than about 0.7 GeV. In the case of the low reheating, an appreciable non-thermal contribution to the WIMP relic density is also necessitated.

KEYWORDS: Cosmology, Dark Matter

PACS CODES: 98.80.Cq, 95.35.+d

CONTENTS

1. INTRODUCTION	1
2. NON-STANDARD COSMOLOGICAL SCENARIA	3
2.1 THE GENERAL SET-UP	3
2.2 THE LOW REHEATING SCENARIO	5
2.3 THE QUINTESSENTIAL KINATION SCENARIO	7
3. THE WIMP RELIC DENSITY	11
3.1 THE BOLTZMANN EQUATION	11
3.2 THE ENHANCEMENT OF $\Omega_\chi h^2$	13
4. PAMELA, ATIC AND FERMI-LAT ANOMALIES	16
4.1 COSMIC RAYS FROM ANNIHILATION OF WIMPs	16
4.2 FITTING THE PAMELA AND ATIC OR FERMI-LAT DATA	18
5. RESTRICTIONS IN THE $m_\chi - \langle\sigma v\rangle$ PLANE	20
5.1 IMPOSED CONSTRAINTS	20
5.2 RESULTS	21
6. CONCLUSIONS	24

1. INTRODUCTION

The accurate determination of cosmological parameters by up-to-date observations, most notably by the *Wilkinson Microwave Anisotropy Probe* (WMAP) [1, 2], establishes a quite extensive and convincing evidence for the constitution of the present universe by an enigmatic component called *Cold Dark Matter* (CDM) with abundance, $\Omega_{\text{CDM}}h^2$, in the following range:

$$\Omega_{\text{CDM}}h^2 = 0.1099 \pm 0.0124 \quad (1.1)$$

at 95% *confidence level* (c.l.). Natural candidates [3] to account for the CDM are [4] the *weakly interacting massive particles* (WIMPs, hereafter denoted as χ) with prominent representative (for other WIMPs, see Ref. [5, 6]) the lightest neutralino [7] which turns out to be the *lightest supersymmetric (SUSY) particle* (LSP) in a sizeable fraction of the parameter space of the SUSY models and therefore, stable under the assumption of the *R-parity* conservation. In view of Eq. (1.1), the relic density of χ 's, $\Omega_\chi h^2$, is to satisfy a very narrow range of values:

$$(a) 0.097 \lesssim \Omega_\chi h^2 \text{ and } (b) \Omega_\chi h^2 \lesssim 0.12, \quad (1.2)$$

with the lower bound being valid under the assumption that CDM is entirely composed by χ 's.

The calculation of $\Omega_\chi h^2$ crucially depends [8] on the adopted assumption about the dominant component of the universe during the decoupling of WIMPs. The usual assumption is that this

occurs during the *radiation dominated* (RD) epoch which commences after the primordial inflation. However, our ignorance about the universal history before *Big Bang nucleosynthesis* (BBN) allows for other possibilities. E.g., the presence of a scalar field, which dominates the budget of the universal energy density through its potential [8, 9, 10, 11, 12, 13] or kinetic [8, 14, 15, 16] energy density, can enhance significantly $\Omega_\chi h^2$ *with respect to* (w.r.t) its value in the *standard cosmology* (SC). In the first case, the scalar field can generate an episode of low reheating which can be accompanied by thermal and/or non-thermal production of χ 's. In the second case, a *kination dominated* (KD) epoch [17], which may be embedded [16, 18, 19, 20, 21] in a quintessential framework, can arise. As a bonus, in the latter case, the problem of the second major component of the present universe, called *Dark Energy* (DE) can be addressed – for reviews see, e.g., Ref. [22].

The aforementioned enhancements of $\Omega_\chi h^2$ have attracted much attention recently [23] since they assist us to interpret, through WIMP annihilation in the galaxy and consistently with Eq. (1.1), the reported [24, 25] excess on the positron (e^+) and/or electron (e^-) *cosmic-ray* (CR) flux, without invoking any pole effect [26], ad-hoc boost factor [27] or other astrophysical sources [28]. In particular, PAMELA experiment has reported [24] (confirming previous experiments [29]) an unexpected rise of e^+ flux fraction for values of the e^+ energy, E_{e^+} , in the range (10 – 100) GeV, in contrast to the power-law falling background. Moreover, data by the ATIC experiment [25] shows an excess in the total e^+ and e^- flux for $300 \leq E_{e^+}/\text{GeV} \leq 800$. On the other hand, the very recently released data from Fermi LAT indicates [30] smaller fluxes than the ATIC data in the same range of energies. Nevertheless, we consider (separately) both latter data in our study.

In this paper we reconsider the increase of $\Omega_\chi h^2$ within a *low reheating scenario* (LRS) or a *quintessential kination scenario* (QKS) in light of the experimental results above. Namely, we recall (Sec. 2) comparatively the salient features of the two non-standard scenaria, solving numerically the relevant system of equations, reviewing the cosmological dynamics and imposing a number of observational constraints. Particularly, in the LRS we consider the late decay of a massive field which reheats the universe to a low reheating temperature. In the QKS, we consider the recently implemented [21] generation of a KD era (associated with an oscillatory evolution of the quintessence field) in the context of tracking quintessential model with a Hubble-induced mass term for the quintessence field. We then (Sec. 3) investigate the enhancement of $\Omega_\chi h^2$ w.r.t its value in SC within these non-standard scenaria. We show that the increase of $\Omega_\chi h^2$ depends on (i) the reheat temperature and the number of χ 's produced per decay and unit mass of the decaying field, in the case of LRS, and (ii) the proximity between the freeze-out temperature and the temperature where the evolution of the quintessence develops extrema, in the case of QKS. We also present (Sec. 4) the energy spectra of the e^\pm -CR, assuming that χ 's annihilate into e^+e^- or $\mu^+\mu^-$ and adopting an isothermal halo profile [31, 32]. Although BBN [32, 33] and *Cosmic Microwave Background* (CMB) [34, 35, 36] tightly constrain the relevant parameters, we achieve rather satisfactory fittings especially to the combination of PAMELA and Fermi-LAT e^\pm -CR data and for the case where χ 's annihilate into $\mu^+\mu^-$ (Sec. 5). Fulfilment of Eq. (1.2) is also possible by appropriately adjusting the parameters of the LRS or QKS. We end up with our conclusions in Sec. 6.

Throughout the text, brackets are used by applying disjunctive correspondence, the subscript or superscript 0 is referred to present-day values (except for the coefficient \bar{V}_0) and \log [\ln] stands for logarithm with basis 10 [e]. Besides Sec. 4, natural units for the Planck's constant, Boltzmann's constant and the velocity of light ($\hbar = c = k_B = 1$) are assumed.

2. NON-STANDARD COSMOLOGICAL SCENARIA

In this section we present comparatively the main features of the two non-standard cosmological scenaria under consideration. Namely, in Sec. 2.1 we expose the basic assumptions of each scenario with reference to the SC and introduce notation. Sec. 2.2 and Sec. 2.3 are devoted to a review of the LRS and QKS respectively. Despite the fact that the displayed scenaria have been already analyzed in Ref. [11, 21] we prefer to briefly recall and update our results for completeness and clarity.

2.1 THE GENERAL SET-UP

According to SC, primordial inflation is followed by a RD era. The χ species (i) are produced through thermal scatterings in the plasma, (ii) reach chemical equilibrium with plasma and (iii) decouple from the cosmic fluid at a temperature $T_F \sim (10 - 20)$ GeV during the RD era. The assumptions above fix the form of the relevant Boltzmann equation, the required strength of the χ interactions for *thermal production* (TP) and lead to an isentropic cosmological evolution during the χ decoupling: The Hubble parameter is $H \propto T^2$ with temperature $T \propto R^{-1}$ where R is the scale factor of the universe. In this context, the $\Omega_\chi h^2$ calculation depends only on two parameters: The χ mass, m_χ and the thermal-averaged cross section of χ times velocity, $\langle\sigma v\rangle$ – see Table 1. Although $\langle\sigma v\rangle$ can be derived from m_χ and the residual (s)particle spectrum once a low energy theory is adopted (see, e.g., Ref. [15]), we treat m_χ and $\langle\sigma v\rangle$ as unrelated input parameters in order to keep our approach as general as possible (see, e.g., Ref. [16, 32]). Also, to be in harmony with the assumptions employed in the derivation of the restrictions mentioned in Sec. 5.1, we consider throughout constant $\langle\sigma v\rangle$'s, i.e., independent of T .

The modern cosmo-particles theories, however, are abundant in scalar massive particles (moduli) which can decay out of equilibrium when H becomes equal to their mass creating episodes of reheating. In the LRS, we assume that such a scalar particle ϕ , with mass m_ϕ , decays with a rate Γ_ϕ into radiation, producing an average number N_χ of χ 's. The key point in this case is that the reheating process is not instantaneous [9, 11]. During its realization, the maximal temperature, T_{\max} , is much larger than the so-called reheat temperature, T_{RH} , which can be taken to be lower than T_F . Also, for $T > T_{RH}$, $H \propto T^4$ with $T \propto R^{-3/8}$ and an entropy production occurs (in contrast with the SC). The χ species (i') decouple during the decaying- ϕ dominated era (ii') do or do not reach chemical equilibrium with the thermal bath (iii') are produced by thermal scatterings and directly by the ϕ decay (which naturally arises even without direct coupling [9]). As a consequence, the $\Omega_\chi h^2$ calculation depends also on T_{RH} , m_ϕ and N_χ – see Table 1.

Another role that a scalar field could play when it does not couple to matter (contrary to ϕ) is this of quintessence. In our QKS, such a scalar field q (not to be confused with the deceleration parameter [2]) is supposed to roll down its inverse power-law potential (with exponent a and a mass scale M) supplemented with a Hubble-induced mass term (with coefficient b) motivated mainly by non-canonical Kähler potential [20, 37] – c.f. Ref. [38]. A mild tuning of b and of the initial conditions at an initial temperature $T_I - H_I = H(T_I)$ and $q_I = q(T_I)$ – ensures the coexistence of an early modified KD phase with the tracking [39, 40] solutions and offers the desirable property of the insensitivity to the initial conditions [20, 21]. Since the q kinetic energy, which decreases as T^6 (except for isolated points) dominates we get $H \propto T^3$ with $T \propto R^{-1}$. If the χ -decoupling occurs during this KD phase – the assumptions (i) and (ii) are maintained – the $\Omega_\chi h^2$ calculation depends also on a, b, M, H_I, T_I and q_I in this scenario – see Table 1.

SC	LRS	QKS
$\bar{\rho}_q = \bar{\rho}_\phi = 0$ $H \propto T^2$ $T \propto R^{-1}$ $sR^3 = \text{cst}$ $N_\chi = 0$	$\bar{\rho}_{\phi_1} \gg \bar{\rho}_{\text{RI}}, \bar{\rho}_q = 0$ $H \propto T^4$ $T \propto R^{-3/8}$ $sR^3 \neq \text{cst}$ $N_\chi \neq 0$	$\bar{\rho}_{q_1} \gg \bar{\rho}_{\text{RI}}, \bar{\rho}_\phi = 0$ $H \propto T^3$ $T \propto R^{-1}$ $sR^3 = \text{cst}$ $N_\chi = 0$
FREE PARAMETERS OF THE $\Omega_\chi h^2$ CALCULATION		
$m_\chi, \langle \sigma v \rangle$	$m_\chi, \langle \sigma v \rangle,$ $T_{\text{RH}}, m_\phi, N_\chi$	$m_\chi, \langle \sigma v \rangle,$ a, b, M, H_1, q_1, T_1

TABLE 1: Comparing the SC with the LRS and the QKS (the various symbols are explained in Sec. 2.1, the subscript I is referred to the onset of each scenario and “cst” stands for “constant”).

In the two non-standard scenaria under consideration, H is given by

$$H^2 = \frac{1}{3m_{\text{P}}^2} \begin{cases} (\rho_\phi + \rho_\chi + \rho_{\text{R}}) & \text{for the LRS,} \\ (\rho_q + \rho_{\text{R}} + \rho_{\text{M}}) & \text{for the QKS,} \end{cases} \quad (2.1)$$

where ρ_i with $i = \phi, q$ and χ is the energy density of ϕ, q and χ respectively and $m_{\text{P}} = M_{\text{P}}/\sqrt{8\pi}$ where $M_{\text{P}} = 1.22 \cdot 10^{19}$ GeV is the Planck mass. The energy density of radiation, ρ_{R} , and the entropy density, s , can be evaluated as a function of T , whilst the energy density of matter, ρ_{M} , with reference to its present-day value:

$$\rho_{\text{R}} = \frac{\pi^2}{30} g_{\rho^*} T^4, \quad s = \frac{2\pi^2}{45} g_{s^*} T^3 \quad \text{and} \quad \rho_{\text{M}} R^3 = \rho_{\text{M}0} R_0^3 \quad (2.2)$$

where $g_{\rho^*}(T)$ [$g_{s^*}(T)$] is the energy [entropy] effective number of degrees of freedom at temperature T . Their precise numerical values are evaluated by using the tables included in public packages [41] and assuming the particle spectrum of the Minimal Supersymmetric Standard Model.

The initial value of H, H_1 , in both non-standard scenaria can be restricted, assuming that a primordial phase of inflation (driven by a scalar field different from ϕ or q , in general) is responsible for the generation of the power spectrum of the curvature scalar P_s and tensor P_t perturbations. Indeed, imposing the conservative restriction $r = P_t/P_s \lesssim 1$ and using the observational [1] normalization of P_s , an upper bound on H_1 can be found as follows:

$$H_1 \lesssim \frac{\pi}{\sqrt{2}} m_{\text{P}} P_{s^*}^{1/2} \Rightarrow H_1 \lesssim 2.65 \cdot 10^{14} \text{ GeV}, \quad (2.3)$$

where $*$ means that P_{s^*} is measured at the pivot scale $k_* = 0.002/\text{Mpc}$.

Let us, finally, introduce a set of normalized quantities which simplify significantly the relevant formulas. In particular we define

$$\bar{\rho}_i = \rho_i/\rho_{\text{c}0}, \quad \text{with } i = \text{R, M, } \phi \text{ and } q, \quad \bar{J} = J/\rho_{\text{c}0}^{3/4} \quad \text{with } J = n_\chi, n_\chi^{\text{eq}} \text{ and } n_\phi, \quad (2.4a)$$

$$\bar{m}_i = m_i/\rho_{\text{c}0}^{1/4} \quad \text{with } i = \chi \text{ and } \phi, \quad \bar{J} = J/H_0 \quad \text{with } J = H \text{ and } \Gamma_\phi \text{ and } \overline{\langle \sigma v \rangle} = \sqrt{3} m_{\text{P}} \rho_{\text{c}0}^{1/4} \langle \sigma v \rangle \quad (2.4b)$$

where n_i with $i = \phi$ and χ is the number density of χ and ϕ respectively. Note that $\rho_\chi = m_\chi n_\chi$ and $\rho_\phi = m_\phi \Delta_\phi n_\phi$ where $\Delta_\phi = (m_\phi - N_\chi m_\chi)/m_\phi$. In our numerical calculation, we use the values:

$$\rho_{\text{c}0} \simeq 8.1 \cdot 10^{-47} h^2 \text{ GeV}^4, \quad \text{with } h = 0.72, \quad \bar{\rho}_{\text{M}0} = 0.26 \quad \text{and} \quad T_0 = 2.35 \cdot 10^{-13} \text{ GeV}. \quad (2.5)$$

We have also $H_0 = 2.13 \cdot 10^{-42} h \text{ GeV}$ and from Eq. (2.2) we get $\bar{\rho}_{\text{R}0} = 8.04 \cdot 10^{-5}$.

2.2 THE LOW REHEATING SCENARIO

We below (Sec. 2.2.1) present the system of equations which governs the cosmological evolution in the LRS, summarize (Sec. 2.2.2) the various observational restrictions that have to be imposed and sketch (Sec. 2.2.3) the basics of the relevant dynamics.

2.2.1 RELEVANT EQUATIONS. Under the assumption that the decay products of ϕ are rapidly thermalized (see below) the energy densities ρ_ϕ and ρ_R obey the following Boltzmann equations

$$\dot{\rho}_\phi + 3H\rho_\phi + \Gamma_\phi\rho_\phi = 0, \quad (2.6a)$$

$$\dot{\rho}_R + 4H\rho_R - \Gamma_\phi\rho_\phi - 2m_\chi\langle\sigma v\rangle\left(n_\chi^2 - n_\chi^{\text{eq}2}\right) = 0, \quad (2.6b)$$

where dot stands for derivative w.r.t the cosmic time, t and n_χ^{eq} is the equilibrium number density of χ , which obeys the Maxwell-Boltzmann statistics:

$$n_\chi^{\text{eq}}(x) = \frac{g}{(2\pi)^{3/2}} m_\chi^3 x^{3/2} e^{-1/x} P_2\left(\frac{1}{x}\right), \quad \text{where } x = \frac{T}{m_\chi} \quad \text{and } P_n(z) = 1 + \frac{(4n^2 - 1)}{8z} \quad (2.7)$$

is obtained by expanding the modified Bessel function of the 2nd kind of order n for $x \ll 1$. Assuming that χ 's are Majorana fermions, we set $g = 2$ for their number of degrees of freedom. Note that although in our numerical program Eqs. (2.6a) and (2.6b) are resolved together with Eq. (3.2) – see Sec. 3.1 –, we here prefer to present just the two first equations since the influence of n_χ to the dynamics of reheating via the last term of the left hand side in Eq. (2.6b) is in general negligible. Moreover, Γ_ϕ can be replaced by T_{RH} through the relation [11]:

$$\Gamma_\phi = 5 \sqrt{\frac{\pi^3 g_{\rho^*}(T_{\text{RH}})}{45} \frac{T_{\text{RH}}^2}{M_{\text{P}}}} = \sqrt{\frac{5\pi^2 g_{\rho^*}(T_{\text{RH}})}{72} \frac{T_{\text{RH}}^2}{m_{\text{P}}}}. \quad (2.8)$$

Note that the adopted prefactor, which is slightly different than those used in the bibliography [10, 12], assists us to approach accurately the numerical solution of $\rho_\phi(T_{\text{RH}}) = \rho_R(T_{\text{RH}})$.

The numerical integration of Eqs. (2.6a) and (2.6b) is facilitated by absorbing the dilution terms. To this end, we find it convenient to define the following variables [10, 11]:

$$f_\phi = \bar{\rho}_\phi R^3, \quad f_R = \bar{\rho}_R R^4, \quad f_\chi = \bar{n}_\chi R^3 \quad \text{and} \quad f_\chi^{\text{eq}} = \bar{n}_\chi^{\text{eq}} R^3. \quad (2.9)$$

and convert the time derivatives to derivatives w.r.t the logarithmic time [11]:

$$\tilde{\tau} = \ln(R/R_I) \Rightarrow R' = R \quad \text{and} \quad R = R_I e^{\tilde{\tau}} \quad (2.10)$$

where prime in this section denotes derivation w.r.t $\tilde{\tau}$ and the value of R_I in this definition can be conveniently selected so as the resolution of the system is numerically stable. Eqs. (2.6a) and (2.6b) become:

$$(a) \quad \bar{H} f'_\phi = -\bar{\Gamma}_\phi f_\phi \quad \text{and} \quad (b) \quad \bar{H} R^2 f'_R = \bar{\Gamma}_\phi f_\phi R^3 + 2\bar{m}_\chi \overline{\langle\sigma v\rangle} (f_\chi^2 - f_\chi^{\text{eq}2}), \quad (2.11)$$

where H and T can be expressed correspondingly, in terms of the variables in Eq. (2.9), as follows:

$$(a) \quad \bar{H} = R^{-3/2} \sqrt{m_\chi f_\chi + f_\phi + f_R/R} \quad \text{and} \quad (b) \quad T = \left(\frac{30 f_R}{\pi^2 g_{\rho^*} R^4 \rho_{\text{c}0}} \right)^{1/4}. \quad (2.12)$$

The system of Eq. (2.11) can be solved from 0 to $\tilde{\tau}_f \sim 50$, imposing the following initial conditions (recall that the subscript I is referred to quantities defined at $\tilde{\tau} = 0$):

$$H_I = m_\phi \Rightarrow \bar{\rho}_{\phi I} = m_\phi^2/H_0^2 \text{ and } \bar{\rho}_{RI} = \bar{\rho}_{\chi I} = 0. \quad (2.13)$$

However, the results on $\Omega_\chi h^2$ do not depend on the explicit value of $\bar{\rho}_{\phi I}$ as long as $T_{RH} < T_F < T_{\max}$, and are invariant [11, 12] for fixed $N_\chi m_\phi^{-1}$ (and T_ϕ , m_χ , $\langle\sigma v\rangle$). Therefore, for presentation purposes, it is convenient to define the following quantity [12]:

$$c_{\chi\phi} = N_\chi \frac{100 \text{ TeV}}{m_\phi}. \quad (2.14)$$

2.2.2 IMPOSED REQUIREMENTS. We impose on the LRS the following requirements:

- The BBN Constraint. The presence of ρ_ϕ should not jeopardize the successful predictions of BBN which commences at about $T_{\text{BBN}} = 1 \text{ MeV}$ [42]. Namely, we require:

$$T_{RH} \geq 1 \text{ MeV} \quad (95\% \text{ c.l.}). \quad (2.15)$$

Given that ϕ decays mostly through gravitational interactions, Γ_ϕ and consequently T_{RH} – see Eq. (2.8) – are highly suppressed. Therefore [12] fulfilment of BBN constraint with more or less natural coupling constants requires $m_\phi \geq 100 \text{ TeV}$.

- Constraints on the range of m_ϕ . Eq. (2.3) assists us to impose an upper bound on m_ϕ due to our initial condition in Eq. (2.13). On the other hand, m_ϕ can be bounded from below, too, demanding the decay of ϕ to a pair of χ 's (with mass m_χ) to be kinematically allowed. All in all we require:

$$2m_\chi \leq m_\phi \lesssim 2.65 \cdot 10^{14} \text{ GeV}. \quad (2.16)$$

Note that the upper bound of Eq. (2.16) assures also the rapid thermalization of the ϕ -decay products. Indeed, the latter condition, which is crucial for Eqs. (2.6a) and (2.6b) to be applicable, is satisfied [43] for $m_\phi \lesssim 8 \cdot 10^{14} \text{ GeV}$.

- Constraint on the range of N_χ . Depending on the coupling between ϕ and χ in a specific theory, a variety of N_χ 's is possible [9, 12, 44]. In our approach we conservatively set the upper bound $N_\chi \leq 1$.

Let us finally mention that, on quite general ground, any modulus ϕ has an unsuppressed coupling to gravitino, \tilde{G} . Possible decay of ϕ to \tilde{G} creates the co-called moduli-induced \tilde{G} problem [44]. To avoid these complications, we are obliged to assume that the masses of \tilde{G} and ϕ are of the same order of magnitude.

2.2.3 THE DYNAMICS OF REHEATING. The cosmological evolution of the various quantities involved in the LRS as a function of $\tilde{\tau}$ is illustrated in Fig. 1 for $m_\phi = 100 \text{ TeV}$ and $(N_\chi, T_{RH}) = (1, 0.5 \text{ GeV})$ (gray lines) or $(N_\chi, T_{RH}) = (7.5 \cdot 10^{-5}, 1 \text{ MeV})$ (light gray lines). In particular, we design $\log \bar{\rho}_i$ with $i = \phi$ (solid lines) and $i = R$ (dashed lines) [T] versus $\tilde{\tau}$ in Fig. 2-(a) [Fig. 2-(b)]. The quantities $\bar{\rho}_i$ with $i = \phi$ and R [T] are computed by substituting the numerical solution of Eq. (2.11) into Eq. (2.9) [Eq. (2.12b)]. From Fig. 1 we can understand the dynamics of the universe during the two distinct phases [10, 11]:

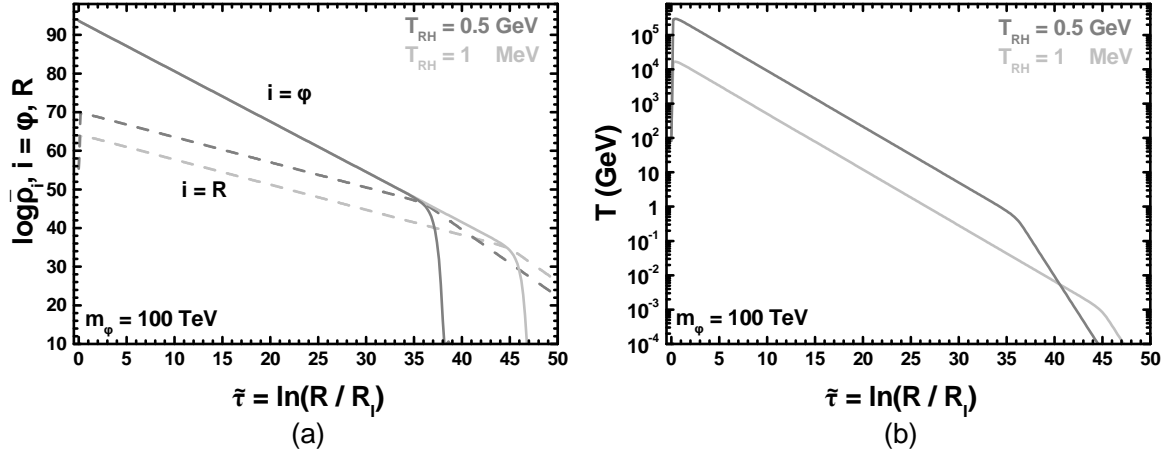


FIGURE 1: The evolution of (a) $\log \bar{\rho}_i$ with $i = \phi$ (solid lines) and R (dashed lines) and (b) T as a function of $\tilde{\tau} = \ln(R/R_1)$ for $m_\phi = 100 \text{ TeV}$ and $(N_\gamma, T_{RH}) = (1, 0.5 \text{ GeV})$ (gray lines) or $(N_\gamma, T_{RH}) = (7.5 \cdot 10^{-5}, 1 \text{ MeV})$ (light gray lines). In both cases, we take $\Omega_\chi h^2 = 0.11$ for $m_\chi = 0.5 \text{ TeV}$ and $\langle \sigma v \rangle = 3 \cdot 10^{-7} \text{ GeV}^{-2}$.

- For $T \gg T_{RH}$, we have $\rho_\phi \gg \rho_R$. Consequently, inserting $\bar{H} \simeq \sqrt{\bar{\rho}_\phi}$ into Eq. (2.11) we extract:

$$(a) \bar{\rho}_\phi = \bar{\rho}_{\phi_1} e^{-3\tilde{\tau}} \quad \text{and} \quad (b) \bar{\rho}_R = \frac{2}{5} \bar{\Gamma}_\phi \bar{\rho}_{\phi_1}^{-1/2} (e^{-3\tilde{\tau}/2} - e^{-4\tilde{\tau}}). \quad (2.17)$$

The function $\bar{\rho}_R(\tilde{\tau})$ reaches at $\tilde{\tau}_{\max} \simeq \ln(1.48) = 0.39$ a maximum value $\bar{\rho}_{R\max} \simeq 0.14 \sqrt{\bar{\rho}_{\phi_1}} \bar{\Gamma}_\phi$ corresponding to a $T = T_{\max}$ derived through Eq. (2.2). The completion of the reheating is realized at $\tilde{\tau} = \tilde{\tau}_{RH}$, such that:

$$\rho_R(\tilde{\tau}_{RH}) = \rho_\phi(\tilde{\tau}_{RH}) \Rightarrow \tilde{\tau}_{RH} \simeq -\frac{2}{3} \ln \frac{2}{5} \bar{\Gamma}_\phi \bar{\rho}_{\phi_1}^{-1/2}. \quad (2.18)$$

where a corner is observed on the curves of Fig. 1-(b).

- For $T < T_{RH}$, we get $\rho_R \gg \rho_\phi$, and so, $\bar{H} \simeq \sqrt{\bar{\rho}_R}$. Plugging it into Eq. (2.11) we can obtain approximately the following expressions:

$$\bar{\rho}_\phi = \bar{\rho}_\phi(\tilde{\tau}_{RH}) \exp\left(-3(\tilde{\tau} - \tilde{\tau}_{RH}) - \frac{5}{4} (e^{2(\tilde{\tau} - \tilde{\tau}_{RH})} - 1)\right) \quad \text{and} \quad \bar{\rho}_R = \bar{\rho}_R(\tilde{\tau}_{RH}) e^{-4(\tilde{\tau} - \tilde{\tau}_{RH})}. \quad (2.19)$$

2.3 THE QUINTESSENTIAL KINATION SCENARIO

We present below (Sec. 2.3.1) the equations which govern the cosmological evolution in the QKS and then enumerate (Sec. 2.3.2) the various observational restrictions that have to be imposed. We also highlight the q dynamics (Sec. 2.3.3) and describe the allowed parameter space (Sec. 2.3.4).

2.3.1 RELEVANT EQUATIONS. Under the assumption that q is spatially homogeneous, it obeys the following Klein-Gordon equation:

$$\ddot{q} + 3H\dot{q} + V_{,q} = 0, \quad \text{where} \quad V = V_a + V_b \quad \text{with} \quad V_a = \frac{M^{4+a}}{q^a} \quad \text{and} \quad V_b = \frac{b}{2} H^2 q^2, \quad (2.20)$$

is the adopted potential for the field q with M a mass-scale and q stands for derivative w.r.t q . In our approach V_b is present throughout the cosmological evolution of q . The induced coupling

between q and CDM during the matter dominated era is too suppressed to have any observational consequence. Nonetheless, we have checked that our results remain intact even if we switch off this term after the onset of the matter domination. The numerical integration of Eq. (2.20) is facilitated by converting the time derivatives to derivatives w.r.t the logarithmic time [16] which is defined as a function of the redshift z :

$$\tau = \ln(R/R_0) = -\ln(1+z). \quad (2.21)$$

Changing the differentiation and introducing the following quantities:

$$\bar{V}_a = V_a/\rho_{c0}, \quad f_q = \dot{q}R^3/\sqrt{\rho_{c0}} \quad \text{and} \quad \bar{q} = q/\sqrt{3}m_{\text{P}}, \quad (2.22)$$

Eq. (2.20) turns out to be equivalent to the system of two first-order equations:

$$f_q = \bar{H}\bar{q}'R^3 \quad \text{and} \quad \bar{H}f_q'/R^3 + b\bar{H}^2\bar{q} + b\bar{H}\bar{H}_{,\bar{q}}\bar{q}^2 + \bar{V}_{a,\bar{q}} = 0, \quad (2.23)$$

$$\text{where} \quad \bar{H}^2 = \frac{1}{1 - b\bar{q}^2/2} \left(\frac{1}{2}f_q^2/R^6 + \bar{V}_a + \bar{\rho}_R + \bar{\rho}_M \right), \quad (2.24)$$

prime in this section denotes derivative w.r.t. τ and M can be found from the dimensionless quantities as follows:

$$M = \left((\sqrt{3}m_{\text{P}})^a \bar{V}_0 \rho_{c0} \right)^{1/(4+a)} \quad \text{with} \quad \bar{V}_a = \bar{V}_0/\bar{q}^a. \quad (2.25)$$

Eq. (2.23) can be resolved numerically if two initial conditions are specified at an initial τ , τ_{I} corresponding to a temperature T_{I} , which is defined as the maximal T after the end of primordial inflation, assuming instantaneous reheating. We take $\bar{q}(\tau_{\text{I}}) = 10^{-2}$ throughout our investigation, without any lose of generality (see below) and let as free parameter $\bar{H}_{\text{I}} = \bar{H}(T_{\text{I}})$.

2.3.2 IMPOSED REQUIREMENTS. Our QKS can be [21] consistent with the following restrictions:

- Constraints on the initial conditions. We focus on the initial conditions which assure a complete initial domination of kination consistently with Eq. (2.3), i.e.,

$$\text{(a) } \Omega_q^{\text{I}} = \Omega_q(T_{\text{I}}) = 1 \quad \text{and} \quad \text{(b) } \bar{H}_{\text{I}} \lesssim 1.72 \cdot 10^{56} \quad (2.26)$$

$$\text{with } \Omega_q = \rho_q/(\rho_q + \rho_R + \rho_M) \quad \text{where } \rho_q = \dot{q}/2 + V. \quad (2.27)$$

- The BBN Constraint. The presence of ρ_q has not to spoil the successful predictions of BBN which commences at about $\tau_{\text{BBN}} = -22.5$ ($T_{\text{BBN}} = 1 \text{ MeV}$) [42]. Namely, we require:

$$\Omega_q^{\text{BBN}} = \Omega_q(\tau_{\text{BBN}}) \leq 0.21 \quad (95\% \text{ c.l.}) \quad (2.28)$$

where 0.21 corresponds to additional effective neutrinos species $\delta N_\nu < 1.6$ [42].

- DE-Density and Coincidence Constraint. These two constraints can be addressed if (i) the present value of ρ_q , ρ_{q0} , is compatible with the abundance of DE in the universe [1] and (ii) ρ_q has already reached the tracking behavior. In other words we have to demand [20]

$$\text{(a) } \Omega_{q0} = \bar{\rho}_{q0} = 0.74 \quad \text{and} \quad \text{(b) } d^2V(\tau=0)/dq^2 \simeq H_0^2, \quad (2.29)$$

where we restrict ourselves to the central experimental value of Ω_{q0} , since, this choice does not affect crucially our results on the CDM abundance.

- Acceleration Constraint. Any successful quintessential model has to account for the present-day acceleration of the universe, i.e., [1] (see also Ref. [45])

$$-1.12 \leq w_q(0) \leq -0.86 \quad (95\% \text{ c.l.}) \quad \text{with} \quad w_q = (\dot{q}^2/2 - V)/(\dot{q}^2/2 + V). \quad (2.30)$$

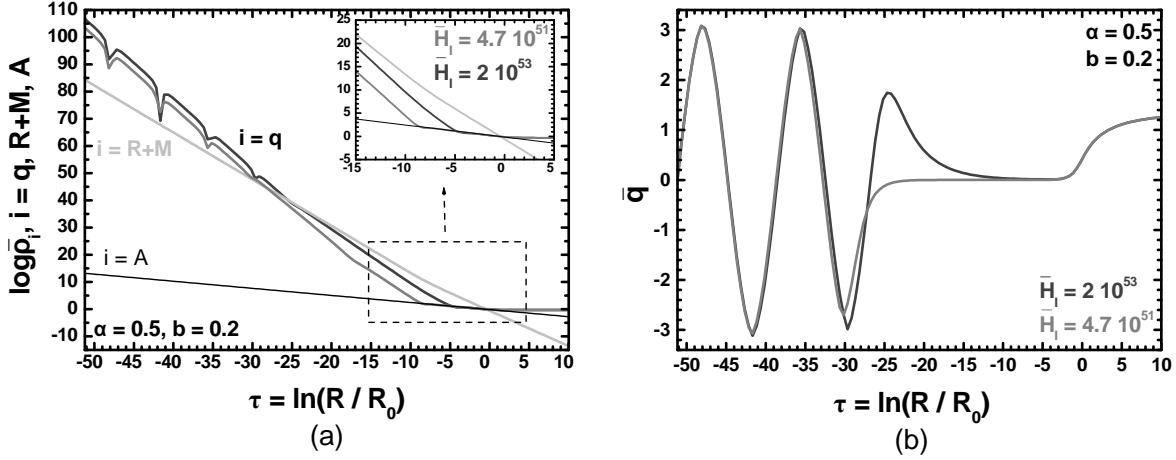


FIGURE 2: The evolution of (a) $\log \bar{\rho}_i$ with $i = q$ (gray [dark gray] line), $R+M$ (light gray line) and A (thick line); and (b) \bar{q} (gray [dark gray] line) as a function of $\tau = \ln(R/R_0)$ for $\bar{q}_I = 0.01$, $a = 0.5$, $b = 0.2$, $T_I = 10^9$ GeV ($\tau_I \approx -51.16$) $M = 4.8$ eV and $\bar{H}_I = 4.7 \cdot 10^{51}$ ($\Omega_q^{\text{BBN}} = 0.0001$) [$\bar{H}_I = 2 \cdot 10^{53}$ ($\Omega_q^{\text{BBN}} = 0.21$)].

2.3.3 THE QUINTESSENTIAL DYNAMICS. The cosmological evolution of the various quantities involved in our QKS as a function of τ is illustrated in Fig. 2 for $\bar{q}_I = 0.01$, $a = 0.5$, $b = 0.2$, $T_I = 10^9$ GeV ($\tau_I \approx -51.2$) $M = 4.8$ eV and $\bar{H}_I = 2 \cdot 10^{53}$ ($\Omega_q^{\text{BBN}} = 0.21$ dark gray lines) or $\bar{H}_I = 2 \cdot 10^{53}$ ($\Omega_q^{\text{BBN}} = 0.0001$, gray lines). Particularly, in Fig. 2-(a) [Fig. 2-(b)] we draw $\log \bar{\rho}_i$ [\bar{q}] versus τ . For $i = q$ (gray and dark gray lines), $\bar{\rho}_q$ is computed by inserting in the last equation of Eq. (2.27) the numerical solution of Eq. (2.23). For $i = R + M$ (light gray line), we show $\bar{\rho}_{R+M} = \bar{\rho}_R + \bar{\rho}_M$ given by Eq. (2.2). For $i = A$ (thin black line), $\bar{\rho}_A$ is the dimensionless energy density of the attractor solution (see below).

From Fig. 2 we can conclude that q undergoes four phases during its cosmological evolution [20, 21, 46]:

- The kinetic-energy dominated phase during which the evolution of both the universe and q is dominated by $\dot{q}/2 \gg V$. Therefore $\bar{H} \approx \bar{H}\bar{q}' / \sqrt{2 - b\bar{q}^2}$ and integrating it we obtain [21]

$$\bar{q} \approx \sqrt{\frac{2}{b}} \sin \sqrt{b}(\tau - \tau_I). \quad (2.31)$$

Obviously, for $b > 0$, q is set in harmonic oscillations during the KD era. In particular, \bar{q} develops extrema at

$$\tau_{\text{ext}} \approx (2k + 1) \sqrt{\frac{1}{b} \frac{\pi}{2}} + \tau_I \quad \text{with } k = 0, 1, 2, \dots \quad (2.32)$$

On the other hand, $\dot{\bar{q}} = \bar{H}\bar{q}'$ almost vanish for $\tau = \tau_{\text{ext}}$. Therefore, at $\tau \approx \tau_{\text{ext}}$, $\bar{\rho}_R$ dominates instantaneously over $\dot{q}/2$. As a consequence, the \bar{q} oscillations become anharmonic. This phase terminates for $\tau = \tau_{\text{KR}}$ where $\rho_q = \rho_R$. For the inputs of Fig. 2 we get $\tau_{\text{KR}} = -25.6$ [$\tau_{\text{KR}} = -28.2$] (or $T_{\text{KR}} = 0.02$ GeV [$T_{\text{KR}} = 0.21$ GeV]) for $\bar{H}_I = 2 \cdot 10^{53}$ [$\bar{H}_I = 4.7 \cdot 10^{51}$]. We observe that the lowest T_{KR} corresponds to the largest \bar{H}_I (and Ω_q^{BBN}). From Fig. 2-(b) we also remark that the height of the fifth peak of \bar{q} decreases with \bar{H}_I . In fact, for $\bar{H}_I < 4.7 \cdot 10^{51}$ we take $\bar{q}_0 < 0$ and so, q can not be served as quintessence (see below).

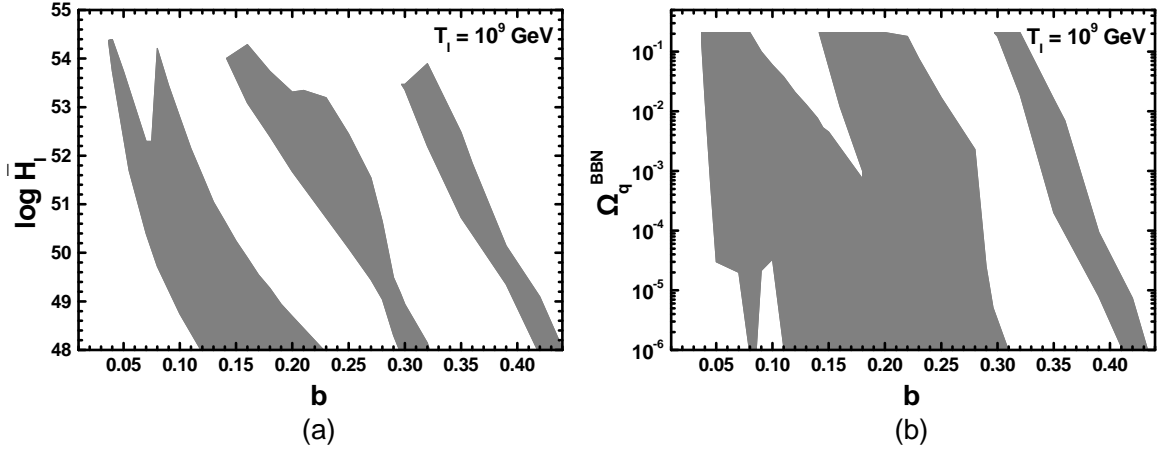


FIGURE 3: Allowed (gray shaded) region by Eqs. (2.26) – (2.30) in the (a) $b - \bar{H}_1$ and (b) $b - \Omega_q^{\text{BBN}}$ plane for $a = 0.5$, $\bar{q}_1 = 0.01$ and $T_1 = 10^9$ GeV.

- The frozen-field dominated phase, where the universe becomes RD and ρ_q is dominated initially by $\dot{q}/2$ and subsequently by V and \bar{q} is stabilized to a constant value – see Fig. 2-(b).
- The attractor dominated phase, where $\rho_q \simeq V$ and ρ_M dominates the evolution of the universe. The system in Eq. (2.20) admits [46] a tracking solution since the energy density of the attractor:

$$\bar{\rho}_A \simeq \bar{\rho}_{Af} \exp\left(-3(1 + w_q^{\text{fp}})(\tau - \tau_{Af})\right) \quad \text{with} \quad w_q^{\text{fp}} = -\frac{2}{a+2} \quad (2.33)$$

tracks $\bar{\rho}_M$ until $\tau = \tau_{Af}$ where the tracking regime terminates and $\bar{\rho}_M \simeq \bar{\rho}_A$. For both \bar{H}_1 's used in Fig. 2, we get $\tau_{Af} = -0.4$ whereas the onset of this phase occurs at $\tau_{Ai} = -4.8$ [$\tau_{Ai} = -8.6$] for $\bar{H}_1 = 2 \cdot 10^{53}$ [$\bar{H}_1 = 4.7 \cdot 10^{51}$]. We observe that although the used \bar{H}_1 's differ by two orders of magnitude, both $\bar{\rho}_q$'s reach $\bar{\rho}_A$ highlighting thereby the insensitivity of our QKS to the initial conditions.

- Vacuum Dominated Phase. For $\tau > \tau_{Af}$, the evolution of the universe is dominated by V . For the parameters used in Fig. 2 we get $w_q(0) \simeq -0.88$ and $\Omega_q(0) \simeq 0.74$.

2.3.4 THE ALLOWED PARAMETER SPACE. The free parameters of our QKS listed in Table 1 can be restricted using the criteria presented in Sec. 2.3.2. Agreement with Eq. (2.30) entails $0 < a \lesssim 0.6$ (compare also with Ref. [47], where less restrictive upper bound on $w_q(0)$ is imposed). The parameter M can be determined for every a through Eq. (2.25) so that Eq. (2.29a) is satisfied. The determination of a and M is independent of τ_1 , \bar{q}_1 and \bar{H}_1 provided that the tracking solution is reached in time. To reduce somehow the parameter space of our investigation we fix $T_1 = 10^9$ GeV (or $\tau_1 = -51.16$). This choice is motivated by the majority of the inflationary models (see, e.g., Ref. [48]). We thereby focus on the two residual free parameters of our model and we design in Fig. 3-(a) [3-(b)] the allowed areas in the $b - \log \bar{H}_1$ [$b - \log \Omega_q^{\text{BBN}}$] plane. In the gray shaded areas Eqs. (2.26) - (2.30) are fulfilled. Obviously our model possesses an allowed parameter space with a band structure. The upper boundary curves of the allowed bands come from Eq. (2.28). Note, however, that saturation of Eq. (2.28) is not possible for $0.08 < b < 0.16$.

For any $(b, \log \bar{H}_1)$, which is consistent with Eq. (2.28) and belongs in a white [gray] band, the resulting \bar{q} after the oscillatory phase turns out to be negative [positive] and so, it cannot [can] be served as quintessence. E.g., let us fix $b = 0.2$. For $51.7 \lesssim \log \bar{H}_1 \lesssim 53.3$, \bar{q} develops five extrema during its evolution – which is of the type shown in – resulting to $\bar{q}_0 > 0$. Actually in Fig. 2-(b) we display the evolution of \bar{q} as a function of τ for the two bounds of this band. As $\log \bar{H}_1$ decreases below 53.3 (where the bound of Eq. (2.28) is saturated), the amplitude of the fifth peak, which appears in the \bar{q} -evolution (at about $\tau \simeq -24.5$) eventually decreases and finally this peak disappears at $\log \bar{H}_1 \simeq 51.7$ where the first allowed band terminates. For $48.7 \lesssim \log \bar{H}_1 \lesssim 51.7$, \bar{q} develops four extremes during its evolution resulting to $\bar{q}_0 < 0$. As $\log \bar{H}_1$ decreases below 51.7 the amplitude of the fourth peak which appears in the \bar{q} -evolution (at about $\tau \simeq -30$) decreases and finally this peak disappears at $\log \bar{H}_1 \simeq 48.7$ where the second allowed band commences. Note that, in the first allowed band, Ω_q^{BBN} increases with \bar{H}_1 but this is not a generic rule.

Variation of T_1 (or equivalently τ_1) modifies the range of the obtainable Ω_q^{BBN} and changes somehow the position of the several bands of our parameter space but do not alter the essential features of our results. E.g., for $b = 0.2$ and $T_1 = 10^{10}$ GeV [$T_1 = 10^8$ GeV] (or $\tau_1 = -53.5$ [$\tau_1 = -48.9$]) the margin of the first allowed band is $53.6 \lesssim \log \bar{H}_1 \lesssim 56.4$ [$49.6 \lesssim \log \bar{H}_1 \lesssim 51.1$] and the second allowed band commences at $\log \bar{H}_1 \simeq 50.7$ [$\log \bar{H}_1 \simeq 46.75$].

3. THE WIMP RELIC DENSITY

We turn to the calculation of the relic density, $\Omega_\chi h^2$, of a WIMP-CDM candidate, χ . Employing the symbols defined in Eq. (2.9), $\Omega_\chi h^2$ can be found from the well-know formula:

$$\Omega_\chi = \frac{\rho_\chi 0}{\rho_{c0}} = \frac{s_0}{\rho_{c0}} \frac{m_\chi n_\chi}{s} \Big|_{\tau_f} \Rightarrow \Omega_\chi h^2 = 4.533 \cdot 10^{-27} \text{ GeV}^2 \frac{m_\chi f_\chi}{sR^3} \Big|_{\tau_f}, \quad (3.1)$$

where $s_0 h^2 / \rho_{c0}^{1/4} = 4.533 \cdot 10^{-27} \text{ GeV}^2$ and τ_f is a value of $\tilde{\tau}$ [τ] for the LRS [QKS] – see Eq. (2.10) [Eq. (2.21)] – large enough so as f_χ is stabilized to its present constant value, $f_{\chi 0}$. Recall that sR^3 in the denominator of Eq. (3.1) remains constant only for $\tilde{\tau} > \tilde{\tau}_{\text{RH}}$ in the LRS but for every τ in the QKS – see Table 1. The evolution of f_χ obeys a Boltzmann equation. In Sec. 3.1 we present and solve this Boltzmann equation and in Sec. 3.2 we investigate how we can achieve within our scenaria an enhancement of $\Omega_\chi h^2$ w.r.t its value in the SC.

3.1 THE BOLTZMANN EQUATION

Since χ 's are in kinetic equilibrium with the cosmic fluid, their number density, n_χ , evolves according to the Boltzmann equation:

$$\dot{n}_\chi + 3Hn_\chi + \langle \sigma v \rangle (n_\chi^2 - n_\chi^{\text{eq}2}) = \begin{cases} \Gamma_\phi N_\chi n_\phi & \text{for the LRS,} \\ 0 & \text{for the QKS,} \end{cases} \quad (3.2)$$

where H is found from Eq. (2.1). In order to find a precise numerical solution to our problem, we have to solve Eq. (3.2) together with Eq. (2.20) [Eqs. (2.6a) and (2.6b)] for the QKS [LRS]. To this end, we rewrite Eq. (3.2) in terms of the quantities defined in Eq. (2.9) as follows

$$\bar{H}R^3 f'_\chi + \overline{\langle \sigma v \rangle} (f_\chi^2 - f_\chi^{\text{eq}2}) = \begin{cases} \bar{\Gamma}_\phi N_\chi \bar{n}_\phi R^6 & \text{for the LRS,} \\ 0 & \text{for the QKS,} \end{cases} \quad (3.3)$$

where \bar{H} given by Eq. (2.12a) [Eq. (2.24)] and prime in this section denotes derivation w.r.t $\tau = \tilde{\tau}$ [$\tau = \tau$] for the LRS [QKS]. Eq. (3.3) can be solved numerically in conjunction with Eq. (2.11) [Eq. (2.23)] for the LRS [QKS]. In the LRS, we use the initial conditions in Eq. (2.13) and we integrate from $\tilde{\tau} = 0$ to $\tilde{\tau}_f \simeq 50$ (with g 's fixed to their values at T_{RH}). In the QKS, we impose the initial condition $\bar{n}_\chi(\tau_\chi) = \bar{n}_\chi^{\text{eq}}(\tau_\chi)$, where τ_χ corresponds to the beginning ($x = 1$) of the Boltzmann suppression of \bar{n}_χ^{eq} in Eq. (2.7). The integration of Eq. (3.3) is realized from τ_I down to $\tau_{\text{BBN}} \simeq -22.5$ (an integration until to 0 gives also the same result).

Based on the semi-analytical expressions of Sec. 2, we can proceed to an approximate computation, which facilitates the understanding of the problem and gives, in most cases, accurate results. In particular, we can set – see Eq. (2.24) [Eqs. (2.17) and (2.18)] for the QKS [LRS]:

$$\bar{H} \simeq \sqrt{\bar{\rho}_R g_C} \quad \text{where} \quad g_C \simeq \begin{cases} 1 + T^4/T_{RH}^4 & \text{for } \tilde{\tau} \ll \tilde{\tau}_{RH}, \\ 1 & \text{for } \tilde{\tau} \gg \tilde{\tau}_{RH} \end{cases} \quad \text{for the LRS, or}$$

$$g_C \simeq \frac{1}{(1 - b\bar{q}^2/2)} \begin{cases} 1 + f_q^2/2R^6\bar{\rho}_R & \text{for } \tau \ll \tau_{KR}, \\ 1 & \text{for } \tau \gg \tau_{KR} \end{cases} \quad \text{for the QKS.} \quad (3.4)$$

Introducing the notion of freeze-out temperature, $T_F = T(\tau_F) = x_F m_\chi$ (see, e.g., Ref. [11, 16] and references therein) we are able to study Eq. (3.3) in the two extreme regimes:

- For $\tau \ll \tau_F$, $f_\chi \simeq f_\chi^{\text{eq}}$. So, it is more convenient to rewrite Eq. (3.3) in terms of the variable $\Delta(\tau) = f_\chi(\tau) - f_\chi^{\text{eq}}(\tau)$ as follows:

$$\bar{H}R^3 \left(\Delta' + f_\chi^{\text{eq}'} \right) + \overline{\langle \sigma v \rangle} \Delta \left(\Delta + 2f_\chi^{\text{eq}} \right) = \begin{cases} \bar{\Gamma}_\phi N_\chi \bar{n}_\phi R^6 & \text{for the LRS,} \\ 0 & \text{for the QKS.} \end{cases} \quad (3.5)$$

The freeze-out point τ_F can be defined by $\Delta(\tau_F) = \delta_F f_\chi^{\text{eq}}(\tau_F)$ where δ_F is a constant of order unity, determined by comparing the exact numerical solution of Eq. (3.3) with the approximate under consideration one. Inserting this definition into Eq. (3.5), we obtain the equation:

$$(\delta_F + 1) f_\chi^{\text{eq}}(\tau_F) \bar{H}R^3 \left(\ln f_\chi^{\text{eq}} \right)'(\tau_F) + \delta_F (\delta_F + 2) \overline{\langle \sigma v \rangle} f_\chi^{\text{eq}2}(\tau_F) = \begin{cases} \bar{\Gamma}_\phi N_\chi \bar{n}_\phi R^6 & \text{for the LRS,} \\ 0 & \text{for the QKS,} \end{cases}$$

$$\text{with } \left(\ln f_\chi^{\text{eq}} \right)'(\tau) = 3 + x' \frac{(16 + 3x)(18 + 25x)}{2x^2(8 + 15x)} \quad (3.6)$$

which can be solved w.r.t τ_F iteratively. The $\tau - x$ [$\tilde{\tau} - x$] dependence can be derived by combining Eq. (2.7) and Eq. (2.2) [Eq. (2.12)] for the QKS [LRS].

- For $\tau \gg \tau_F$, $f_\chi \gg f_\chi^{\text{eq}}$ and so, we can set $f_\chi^2 - f_\chi^{\text{eq}2} \simeq f_\chi^2$ in Eq. (3.3). Let us analyze this case for each scenario separately:

◆ In the LRS and for the range of the parameters under consideration – see Sec. 3.2 – we single out two cases:

- * *Dominant non-thermal production* (non-TP). In this case, which is mainly applicable for very low T_{RH} 's, $f_\chi^2 \overline{\langle \sigma v \rangle} \ll \bar{\Gamma}_\phi N_\chi \bar{n}_\phi R^6$. Therefore, Eq. (3.3) can be integrated analytically inserting into it Eq. (2.17a) as follows:

$$f_{\chi 0} \simeq \frac{2}{3} \sqrt{\bar{\rho}_{\phi 1}} \bar{\Gamma}_\phi N_\chi \Delta_\phi^{-1} \bar{m}_\phi^{-1} \left(e^{3\tilde{\tau}_{RH}/2} - e^{3\tilde{\tau}_F/2} \right). \quad (3.7)$$

Since $f_{\chi 0}$ takes its main contribution close to $\tilde{\tau}_{RH} \gg \tilde{\tau}_F$ our result is more or less independent of $\tilde{\tau}_F$.

* Equipartition between TP and non-TP. Besides f_χ^{eq} none of the other terms of Eq. (3.3) can be neglected in this case. A rather precise result for $f_{\chi 0}$ can be obtained by numerically integrating Eq. (3.3) subsequently from (i) $\tilde{\tau} = \tilde{\tau}_F$ until $\tilde{\tau} = \tilde{\tau}_{\text{RH}}$ with initial condition $f_\chi(\tilde{\tau}_F) = (\delta_F + 1)f_\chi^{\text{eq}}(\tilde{\tau}_F)$ and using $\bar{H}[\bar{\rho}_\phi]$ given by Eq. (3.4) [Eq. (2.17a)]; (ii) $\tilde{\tau} = \tilde{\tau}_{\text{RH}}$ until $\tilde{\tau} = \tilde{\tau}_f \simeq 50$, employing the estimates of Eq. (2.19) for $\bar{\rho}_\phi$ and $\bar{\rho}_R$. A less accurate result for this case can be derived [9, 10] by equating the annihilation rate $\Gamma_\chi = n_\chi \langle \sigma v \rangle$ to the expansion rate H at the completion of reheating. Combining Eq. (2.17a) and Eq. (2.18) we obtain $\bar{H}(\tilde{\tau}_{\text{RH}}) = 2\bar{\rho}_\phi(\tilde{\tau}_{\text{RH}}) = 2\sqrt{2}\bar{\Gamma}_\phi/5$ and so, we arrive at:

$$\frac{n_\chi}{s} \simeq \frac{9\sqrt{2}}{\pi^2} \frac{\Gamma_\phi}{\langle \sigma v \rangle T_{\text{RH}}^3} \quad (3.8)$$

In general, this result underestimates the numerical one by a factor of unity. However, the method applied reveals the presence of the phenomenon of reannihilation [49] in this case, i.e., the occurrence of a secondary (for $\tilde{\tau} \gg \tilde{\tau}_F$) χ decoupling – see Sec. 3.2.1.

◆ In the QKS, we can integrate numerically Eq. (3.3) from τ_F down to 0, as follows:

$$f_{\chi 0} = \left(f_{\chi F}^{-1} + J_F \right)^{-1}, \quad \text{where } J_F = \int_{\tau_F}^0 d\tau \frac{\overline{\langle \sigma v \rangle}}{\bar{H}R^3} \quad \text{and } f_{\chi F} = (\delta_F + 1) f_\chi^{\text{eq}}(\tau_F). \quad (3.9)$$

Although not crucial, a choice $\delta_F = 1.2 \mp 0.2$ assists us to approach better the precise numerical solution of Eq. (3.3).

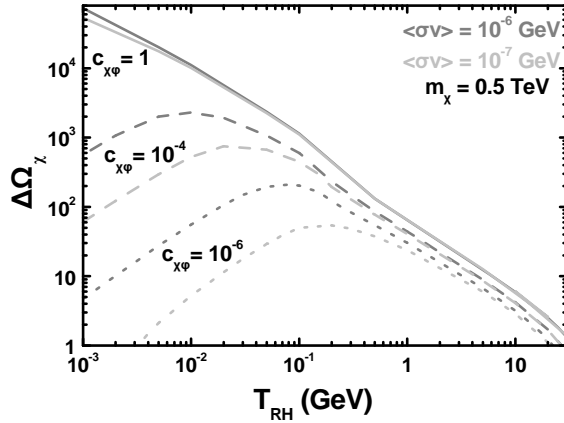
3.2 THE ENHANCEMENT OF $\Omega_\chi h^2$

As we explain in Sec. 4 the interpretation of the e^\pm -CR anomalies favors $10^{-7} \lesssim \langle \sigma v \rangle / \text{GeV}^{-2} \lesssim 10^{-6}$ which results to $0.0025 \gtrsim \Omega_\chi h^2|_{\text{SC}} \gtrsim 0.00027$ for $0.1 \leq m_\chi / \text{TeV} \leq 3$, where $\Omega_\chi h^2|_{\text{SC}}$ denotes $\Omega_\chi h^2$ within the SC. Clearly, the resulting $\Omega_\chi h^2|_{\text{SC}}$ lie much lower than the range of Eq. (1.2). However, the proposed non-standard scenaria can increase $\Omega_\chi h^2$ w.r.t $\Omega_\chi h^2|_{\text{SC}}$. The resulting enhancement can be quantified, by defining the quantity:

$$\Delta\Omega_\chi = \left(\Omega_\chi h^2 - \Omega_\chi h^2|_{\text{SC}} \right) / \Omega_\chi h^2|_{\text{SC}}. \quad (3.10)$$

We below analyze the behavior of $\Delta\Omega_\chi$ as a function of the free parameters of each non-standard scenario separately.

3.2.1 THE LRS. Let us initially clarify that in the LRS, both signs of $\Delta\Omega_\chi$ are possible, as emphasized in Ref. [11, 12]. However, we here confine ourselves to the combination of parameters which assure the favored from the e^\pm -CR data $\Delta\Omega_\chi > 0$. The dependence of $\Delta\Omega_\chi$ on the free parameters of the LRS can be inferred from Fig. 4, where we depict $\Delta\Omega_\chi$ versus T_{RH} for $m_\chi = 0.5 \text{ TeV}$, $\langle \sigma v \rangle = 10^{-6} \text{ GeV}^{-2}$ [$\langle \sigma v \rangle = 10^{-7} \text{ GeV}^{-2}$] (gray [light gray] lines) and $c_{\chi\phi} = 1$ (solid lines), $c_{\chi\phi} = 10^{-4}$ (dashed lines) and $c_{\chi\phi} = 10^{-6}$ (dotted lines). The ranges of parameters where each production mechanism is activated are also shown in the table included. Note that the exposed ranges depend very weakly on the employed m_χ 's and $\langle \sigma v \rangle$'s. We observe that $\Delta\Omega_\chi$ increases with T_{RH} when we have non-TP as expected from Eq. (3.7), but it decreases as T_{RH} increases when we have equipartition between non-TP and TP, as anticipated in Eq. (3.8). The former mechanism is dominant mainly for very low T_{RH} 's whereas the latter is present for higher T_{RH} 's. The accuracy



$c_{\chi\phi}$	T_{RH} (GeV)	χ PRODUCTION
10^{-6}	0.001 – 0.2	NON-TP
	0.2 – 30	NON-TP + TP
10^{-4}	0.001 – 0.02	NON-TP
	0.02 – 30	NON-TP + TP
1	0.001 – 30	NON-TP+TP

FIGURE 4: $\Delta\Omega_\chi$ versus T_{RH} for the LRS with $m_\chi = 0.5$ TeV, $\langle\sigma v\rangle = 10^{-6}$ GeV $^{-2}$ [$\langle\sigma v\rangle = 10^{-7}$ GeV $^{-2}$] (gray [light gray] lines) and $c_{\chi\phi} = 1$ (solid lines), $c_{\chi\phi} = 10^{-4}$ (dashed lines) and $c_{\chi\phi} = 10^{-6}$ (dotted lines). In the table we also show the type of the χ production for each $c_{\chi\phi}$ and the various ranges of T_{RH} .

of the corresponding empirical expressions in Eq. (3.7) [Eq. (3.8)] increases as T_{RH} decreases [increases] and as $\langle\sigma v\rangle$ decreases [increases]. It is remarkable that for $c_{\chi\phi}$'s where both production mechanisms are possible (e.g., $c_{\chi\phi} = 10^{-6}$ or 10^{-4}) we can obtain the same $\Delta\Omega_\chi$ for two values of T_{RH} . In general, $\Delta\Omega_\chi$ increases with N_χ . Augmentation of m_χ increases $\Omega_\chi h^2$, too, but does not alter the dependence of $\Omega_\chi h^2$ on T_{RH} and the ranges where the χ -production mechanisms are activated.

The operation of the two types of χ production encountered in Fig. 4 is visualized in Fig. 5-(a) and (b). In these, we display the actual χ yield, n_χ/s (solid lines) and its equilibrium value, n_χ^{eq}/s (dashed lines) the dimensionless actual interaction rate of χ , $\bar{\Gamma}_\chi = \bar{n}_\chi \langle\sigma v\rangle$ (solid lines), its equilibrium value, $\bar{\Gamma}_\chi^{eq} = \bar{n}_\chi^{eq} \langle\sigma v\rangle$ (dotted lines) and the dimensionless expansion rate \bar{H} (dashed lines) – given by Eq. (2.12a) – versus $\tilde{\tau}$. In both figures we use $m_\chi = 0.5$ TeV, $m_\phi = 100$ TeV, $\langle\sigma v\rangle = 3 \cdot 10^{-7}$ GeV $^{-2}$ and $(N_\chi, T_{RH}) = (1, 0.5$ GeV) [$(N_\chi, T_{RH}) = (7.5 \cdot 10^{-5}, 1$ MeV)] (gray [light gray] lines). For the selected parameters, the evolution of the background energy densities ($\log \bar{\rho}_\phi$ and $\log \bar{\rho}_R$) and T is presented in Fig. 1-(a) and (b). The completion of reheating occurs at $\tilde{\tau}_{RH} \approx 36.1$ [$\tilde{\tau}_{RH} = 45.1$] for $T_{RH} = 0.5$ GeV [$T_{RH} = 1$ MeV].

From Fig. 5-(a) we can deduce that n_χ/s takes its present value close to [clearly above] $\tilde{\tau}_{RH}$ for $T_{RH} = 1$ MeV [$T_{RH} = 0.5$ GeV]. For this reason, the integration of Eq. (3.3) until $\tilde{\tau}_{RH}$ for non-TP is sufficient for an accurate result – see Eq. (3.7) –, but insufficient when non-TP and TP interplay. The χ reannihilation takes place along the almost vertical part of the gray line for $\tilde{\tau}$ a little lower than $\tilde{\tau}_{RH}$. It is notable that in Ref. [11, 12] which focus on lower $\langle\sigma v\rangle$'s than the ones considered here, the phenomenon of reannihilation is not stressed.

This effect is further analyzed, following the approach of the first paper in Ref. [49], in Fig. 5-(b). From this we infer that for $T_{RH} = 1$ MeV, where non-TP outstrips, χ decouples from plasma only once at $\tilde{\tau}_F = 16.5$ where $\Gamma_\chi = \Gamma_\chi^{eq} = H$ and an intersection of the light gray lines is observed (note that the light gray and gray dashed lines coincide at that region). On the contrary, for $T_{RH} = 0.5$ GeV, where non-TP and TP coexist, we observe that χ decouples from plasma initially at about $\tilde{\tau}_F = 26.3$ where $\Gamma_\chi^{eq} = H$ but also at $\tilde{\tau}_{F2} = 37.9 > \tilde{\tau}_{RH}$ where $\Gamma_\chi = H$. In other words, we observe two intersections between the two pairs of the three gray lines. This effect signalizes the existence

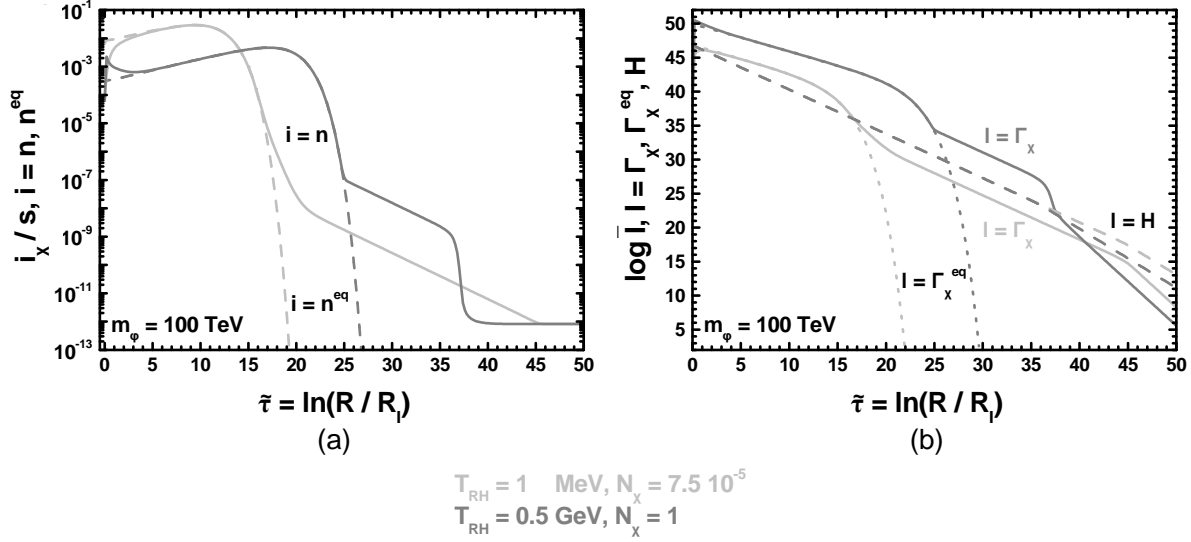


FIGURE 5: (a) n_{χ}/s (solid lines) and n_{χ}^{eq}/s (dashed lines) versus $\tilde{\tau}$ and (b) $\bar{\Gamma}_{\chi}$ (solid lines), $\bar{\Gamma}_{\chi}^{\text{eq}}$ (dotted lines) and \bar{H} (dashed lines) versus $\tilde{\tau}$ for the LRS with $m_{\chi} = 0.5 \text{ TeV}$, $m_{\phi} = 100 \text{ TeV}$, $\langle\sigma v\rangle = 3 \cdot 10^{-7} \text{ GeV}^{-2}$ and $(N_{\chi}, T_{RH}) = (1, 0.5 \text{ GeV})$ [$(N_{\chi}, T_{RH}) = (7.5 \cdot 10^{-5}, 1 \text{ MeV})$] (gray [light gray] lines) – in both cases, we get $\Omega_{\chi} h^2 = 0.11$.

of a period of χ reannihilation similar to that noticed in Ref. [49]. Contrary to that situation, in our case (i) Γ_{χ} remains larger than H after the first χ decoupling and drops sharply below H after reannihilation, and (ii) H smoothly evolves from its behavior during LRS to that within RD era.

3.2.2 THE QKS. The presence of $g_C > 1$ in Eq. (3.6) and, mainly, in Eq. (3.9) reduces J_F w.r.t its value in the SC generating, thereby, $\Delta\Omega_{\chi} > 0$ within the QKS. The mechanism of the χ decoupling in this case, for both $b = 0$ and $b \neq 0$, is pretty known – see Ref. [8, 14, 16]. However, a peculiar effect emerges in the dependence of $\Delta\Omega_{\chi}$ on m_{χ} for $b \neq 0$ which can be inferred from Fig. 6, where we display $\Delta\Omega_{\chi}$ versus m_{χ} for $a = 0.5$, $\bar{H}_I = 6.3 \cdot 10^{53}$, $\langle\sigma v\rangle = 10^{-6} \text{ GeV}^{-2}$ [$\langle\sigma v\rangle = 10^{-7} \text{ GeV}^{-2}$] (gray [light gray] lines) and $b = 0$ (solid lines), $b = 0.15$ (dashed lines) and $b = 0.32$ (dotted lines). The chosen \bar{H}_I 's result to $\Omega_q^{\text{BBN}} \simeq 0.01, 0.068$ or 0.19 for $b = 0, 0.15$ or 0.32 correspondingly.

Obviously, for $b = 0$ we get a pure KD era and our results reduce to those presented in Ref. [16], i.e., $\Delta\Omega_{\chi}$ increases when m_{χ} increases or $\langle\sigma v\rangle$ decreases. On the contrary, for $b \neq 0$, $\Delta\Omega_{\chi}$ depends crucially on the hierarchy between τ_F and τ_{ext} found from Eqs. (3.6) and (2.32) respectively. Given that J_F takes its main contribution from g_C for $\tau \sim \tau_F$, J_F is enhanced – see Eq. (3.9) – if τ_F is lower than τ_{ext} and close to it, since g_C is suppressed ($g_C \simeq 1$) for $\tau \simeq \tau_{\text{ext}}$. As a consequence – see Eqs. (3.1) and (3.9) – $\Delta\Omega_{\chi}$ diminishes. This argument is highlighted in the table of Fig. 6. There, we list the range of τ_F for $0.1 \leq m_{\chi}/\text{TeV} \leq 3$ and $\langle\sigma v\rangle = 10^{-7} \text{ GeV}^{-2}$ or $\langle\sigma v\rangle = 10^{-6} \text{ GeV}^{-2}$ and the logarithmic time τ_{ext} at which the closest to τ_F 's peak in the q evolution takes place for $b = 0.15$ or $b = 0.32$ and $\bar{H}_I = 6.3 \cdot 10^{53}$. Clearly τ_F [τ_{ext}] is independent of b and \bar{H}_I [m_{χ} and $\langle\sigma v\rangle$]. As m_{χ} increases above 0.1 TeV , τ_F moves closer to τ_{ext} and $\Delta\Omega_{\chi}$ decreases with its minimum $\Delta\Omega_{\chi}|_{\text{min}}$ occurring at $\tau_F^{\text{min}} \simeq \tau_{\text{ext}}$. The small deviation of τ_F^{min} from τ_{ext} can be attributed to the presence of $f_{\chi F}$ in Eq. (3.9). The appearance of the minima can be avoided if τ_F 's happen to remain constantly lower than τ_{ext} 's – see, e.g., Fig. 8-(c₂). Variation of T_I or \bar{H}_I leads to a displacement of τ_{ext} 's – see Eq. (2.32) – relocating, thereby, the minima of $\Delta\Omega_{\chi}$ in Fig. 6. However, our conclusions on the behavior of $\Delta\Omega_{\chi}$ remain intact.

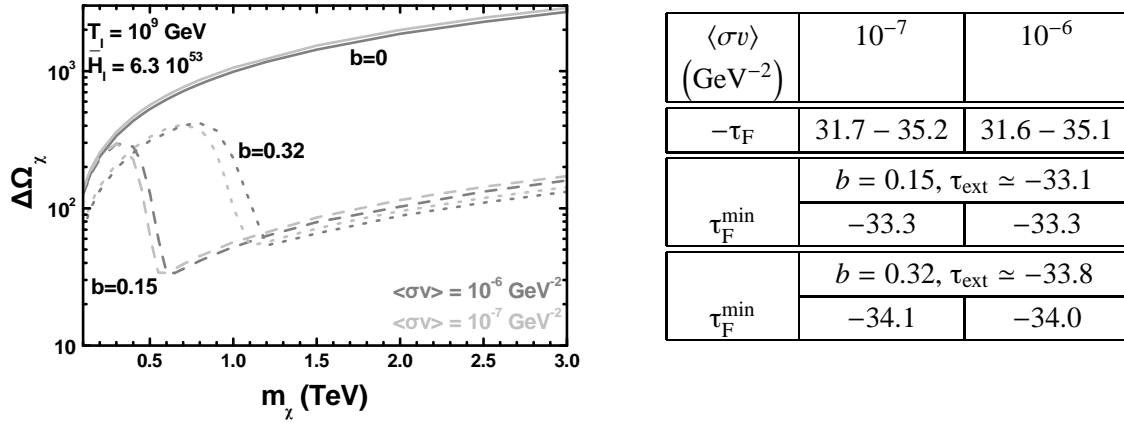


FIGURE 6: $\Delta\Omega_\chi$ versus m_χ for the QKS with $a = 0.5$, $\bar{H}_1 = 6.3 \cdot 10^{53}$, $T_1 = 10^9$ GeV, $\langle\sigma v\rangle = 10^{-6}$ GeV⁻² [$\langle\sigma v\rangle = 10^{-7}$ GeV⁻²] (gray [light gray] lines) and $b = 0$ (solid lines), $b = 0.15$ (dashed lines) and $b = 0.32$ (dotted lines). In the table we also show the range of τ_F for $0.1 \leq m_\chi/\text{TeV} \leq 3$, the freeze-out logarithmic time τ_F^{\min} at which the minima of $\Delta\Omega_\chi$ occur and the closest to τ_F^{\min} 's τ_{ext} 's for the selected b 's.

4. PAMELA, ATIC AND FERMI-LAT ANOMALIES

The aforementioned $\Delta\Omega_\chi$ obtained within the LRS or QKS assists us to explain the experimental data on the e^\pm -CRs consistently with Eq. (1.2). Indeed, the observed anomalies on the CR e^\pm fluxes can be attributed to the annihilation of χ 's in the galaxy provided that m_χ and $\langle\sigma v\rangle$ are chosen appropriately. In Sec. 4.1 we outline the basic formalism that we employ in order to estimate the observable quantities as a function of these parameters and in Sec. 4.2 we display our fittings.

4.1 COSMIC RAYS FROM ANNIHILATION OF WIMPS

After being produced in the Milky Way halo, charged CRs propagate in the galaxy and its vicinity in a rather complicated way before reaching the earth. Their propagation is commonly evaluated by solving a diffusion equation [50, 51] with static cylindrical boundary conditions. The solution can be casted into the following semi-analytical form [50, 51, 52] which yields the e^+ flux per energy – in units GeV⁻¹cm⁻²s⁻¹sr⁻¹ – at earth from the χ annihilation:

$$\Phi_{e^+}^{\chi\chi}(E) = \frac{1}{2} \frac{v_{e^+}}{4\pi b(E)} \left(\frac{\rho_\odot}{m_\chi} \right)^2 \langle\sigma v\rangle \int_E^{m_\chi} dE' I(\lambda_D(E, E')) \frac{dN_{e^+}}{dE'_{e^+}}, \quad (4.1)$$

where v_{e^+} is the velocity of e^+ which is practically equal to this of the light, the pre-factor of 1/2 arises from our assumption that χ is a Majorana particle, $\rho_\odot = 0.3$ GeV/cm³ is the local CDM density, $b(E) = E^2/(\text{GeV } t_E)$ with $t_E = 10^{16}$ s is the energy loss rate function and dN_{e^+}/dE'_{e^+} denotes the energy distribution of e^+ 's per χ annihilation. Motivated by the highly restrictive PAMELA data [53] on the anti-proton mode of the CDM annihilation, we consider a purely leptophilic χ (however, see also Ref. [54]). In particular, we consider χ annihilating to e^-e^+ or $\mu^-\mu^+$ since both cases can be reconciled [32] with the present bounds imposed from BBN (see Sec. 5.1.2). In the first case, dN_{e^+}/dE'_{e^+} is given simply in terms of the Dirac delta distribution [55]. In the second case, we use an analytic parametrization of dN_{e^+}/dE'_{e^+} (presented in Ref. [56]) which reproduces

quite accurately the numerical outputs of the package PYTHIA [57]. Namely, we take

$$\frac{dN_{e^+}}{dE_{e^+}} = \begin{cases} \delta(E_{e^+} - m_\chi) & \text{for } \chi\chi \rightarrow e^+e^-, \\ (\alpha_{\text{em}}/\pi)A \exp[-(A_1y + A_1y^2)] + B_1 + B_2y & \text{for } \chi\chi \rightarrow \mu^+\mu^-, \end{cases} \quad (4.2)$$

where α_{em} is the fine-structure constant computed at a scale equal to $2m_\chi$, $0 < y = E_{e^+}/m_\chi \leq 1$ and $J = \tilde{J}(m_\chi/0.5 \text{ TeV})^{\delta_J}$ with $J = A, A_1, A_2, B_1, B_2$ and

$$\begin{aligned} (\tilde{A}, \tilde{A}_1, \tilde{A}_2, \tilde{B}_1, \tilde{B}_2) &= (-0.296635, 2.65121, 14.8445, 0.0042505, -0.00427157), \\ (\delta_A, \delta_{A_1}, \delta_{A_2}, \delta_{B_1}, \delta_{B_2}) &= (-1.01424, 0.017198, -0.0107585, -0.999819, -0.999819). \end{aligned}$$

Also, $I(\lambda_D)$ is the dimensionless halo function which fully encodes the galactic astrophysics with $\lambda_D(E, E')$ the diffusion length from energy E to energy E' which is given by

$$\lambda_D^2 = 4K_0 t_E \left[\frac{(E'/\text{GeV})^{\delta-1} - (E/\text{GeV})^{\delta-1}}{\delta-1} \right]. \quad (4.3)$$

To compute $I(\lambda_D)$ we employ the semi-empirical function proposed in Ref. [52, 55]. Namely,

$$I(\lambda_D) = a_0 + a_1 \tanh\left(\frac{b_1 - l}{c_1}\right) \left[a_2 \exp\left(-\frac{(l - b_2)^2}{c_2}\right) + a_3 \right] \quad \text{with } l = \log\left(\frac{\lambda_D}{\text{kpc}}\right). \quad (4.4)$$

The involved in Eqs. (4.3) and (4.4) constants [52] depend on the CDM distribution and the propagation model that we consider. As we emphasize in Sec. 5.1.4, the constraint from the γ CRs enforces us to adopt the isothermal halo profile [58] which weakens the relative restrictions. Note, however, that our results on $\Phi_{e^+}^{\chi\chi}$ are quite close to those that we would had obtained if we had used the NFW halo [59] profile – c.f. Ref. [31, 52]. We also use the MED propagation model which provides better fits to the experimental data compared with those of MIN (M2) model - in accordance with Ref. [55]. Note that only these two propagation models are consistent [51] with the observed boron-to-carbon ratio in the CR flux. Therefore, we use [52] throughout

$$(a_0, a_1, a_2, a_3, b_1, b_2, c_1, c_2) = (0.495, 0.629, 0.137, 0.784, 0.766, 0.55, 0.193, 0.296)$$

and $(K_0, \delta) = (0.0112 \text{ kpc}^2/\text{My}, 0.7)$. We explicitly verified that the numerically fitted function in Eq. (4.4) reproduces quite accurately and fast enough the results obtained by performing numerically the relevant integrations presented in the earlier formulae of Ref. [51]. Moreover, the formalism of Ref. [52] overcomes successfully the mismatching problem (in the numerical integration) which is mentioned in Ref. [60].

In order to calculate the total fluxes, we also have to estimate the background e^\pm fluxes. In our study, we take into account the fluxes of (i) secondary e^+ ($\Phi_{e^+}^{\text{sec}}$) produced by collisions between primary protons and interstellar medium in our galaxy (ii) primary e^- ($\Phi_{e^-}^{\text{prim}}$) presumably produced in supernova remnants and (iii) secondary e^- ($\Phi_{e^-}^{\text{sec}}$) produced by spallation of CRs in the interstellar medium. These fluxes are commonly parameterized as [50]

$$\Phi_{e^+}^{\text{sec}} = \frac{4.5 (E/\text{GeV})^{0.7}}{1 + 650 (E/\text{GeV})^{2.3} + 1500 (E/\text{GeV})^{4.2}}, \quad (4.5a)$$

$$\Phi_{e^-}^{\text{prim}} = \frac{0.16 (E/\text{GeV})^{-1.1}}{1 + 11 (E/\text{GeV})^{0.9} + 3.2 (E/\text{GeV})^{2.15}}, \quad (4.5b)$$

$$\Phi_{e^-}^{\text{sec}} = \frac{0.7 (E/\text{GeV})^{0.7}}{1 + 110 (E/\text{GeV})^{1.5} + 600 (E/\text{GeV})^{2.9} + 580 (E/\text{GeV})^{4.2}}, \quad (4.5c)$$

in units $\text{GeV}^{-1}\text{cm}^{-2}\text{s}^{-1}\text{sr}^{-1}$. With these backgrounds, the total e^\pm fluxes read

$$\Phi_{e^+} = \Phi_{e^+}^{\chi\chi} + \Phi_{e^+}^{\text{sec}} \quad \text{and} \quad \Phi_{e^-} = \Phi_{e^-}^{\chi\chi} + c_{e^-} \Phi_{e^-}^{\text{prim}} + \Phi_{e^-}^{\text{sec}} \quad (4.6)$$

where $\Phi_{e^-}^{\chi\chi} = \Phi_{e^+}^{\chi\chi}$ and $c_{e^-} \simeq (0.6 - 0.8)$ is a normalization factor. We take $c_{e^-} = 0.6$ [$c_{e^-} = 0.7$] so that our flux calculation is consistent with the ATIC [Fermi-LAT] data in the low energy range of (20 – 70) GeV [55].

4.2 FITTING THE PAMELA AND ATIC OR FERMI-LAT DATA

Using the fluxes defined above, we can evaluate the observable quantities and compare them with the experimental outputs. In order to qualify our fittings to the experimental data, we perform a χ^2 analysis. In particular, we define the χ^2 variables as [55, 56, 60]

$$\chi_A^2 = \sum_{i=1}^{N_A} \frac{(F_{Ai}^{\text{obs}} - F_{Ai}^{\text{th}})^2}{(\Delta F_{Ai}^{\text{obs}})^2}, \quad \text{with} \quad F_A = \begin{cases} \Phi_{e^+} / (\Phi_{e^+} + \Phi_{e^-}) & \text{and } N_A = 7 \text{ for } A = 1, \\ E_{e^+}^3 (\Phi_{e^+} + \Phi_{e^-}) & \text{and } N_A = \begin{cases} 21 & \text{for } A = 2, \\ 26 & \text{for } A = 3, \end{cases} \end{cases} \quad (4.7)$$

where $A = 1, 2, 3$ stands for the PAMELA [24], ATIC [25] or Fermi-LAT [30] data respectively which are considered as independent sets. The index i runs over the data points of each experiment A , the superscript ‘‘obs’’ [‘‘th’’] refers to measured [theoretically predicted] quantities whereas ΔF^{obs} means error in the experimentally observable F . N_A is the number of data points considered from the experiment A . Note that, from the PAMELA data-set, we use [55, 56] only the 7 data points above 9.1 GeV where the effect of solar modulation is expected to be small. In our analysis we take into account only the vertical errors. We also conservatively combine, independently for each data-point, in quadrature statistical and systematic errors released from Fermi LAT [30].

In Fig. 7 we show the predicted observable quantities compared to the experimental data as a function of the e^+ energy E_{e^+} , assuming χ annihilating to e^+e^- (dot-dashed lines) or $\mu^+\mu^-$ (dashed lines). We use the best-fit $(m_\chi, \langle\sigma v\rangle)$ ’s obtained from minimization of $\chi_1^2 + \chi_2^2$ [$\chi_1^2 + \chi_3^2$] in Fig. 7-(a₁) and (a₂) [Fig. 7-(b₁) and (b₂)]. Since ATIC and Fermi-LAT data are not consistent with each other, we do not combine them but present results using only either of the two. The relevant $(m_\chi, \langle\sigma v\rangle)$ ’s can be read in the Table 2 together with the corresponding $\chi^2/\text{d.o.f}$, where d.o.f denotes the number of degrees of freedom involved in our fits which is equal to $N_1 + N_2 - 2 = 26$ [$N_1 + N_3 - 2 = 31$] for PAMELA and ATIC [PAMELA and Fermi-LAT] data (2 is the number of the fitting variables, m_χ and $\langle\sigma v\rangle$). As can be deduced from Table 2, an exceptionally good fit to PAMELA and Fermi-LAT data arises for χ annihilating to $\mu^+\mu^-$, whereas in the other cases the fits are rather poor since we get just $\chi^2/\text{d.o.f} \simeq 2.5 - 3$ for 28 or 33 data points. Better fits can be probably attained under the assumption that χ ’s both annihilate and decay, as pointed out in Ref. [55].

In Table 2 we also list the maximal $\langle\sigma v\rangle$, $\langle\sigma v\rangle_{\text{max}}$, allowed by Eq. (5.4) (see Sec. 5.1.3) and the resulting $\Omega_\chi h^2|_{\text{SC}}$ ’s. It is remarkable that $\Omega_\chi h^2|_{\text{SC}}$ turns out to be well below the range of Eq. (1.2) implied by the CDM considerations. As a consequence, the SC can not be consistent with the interpretation of the e^\pm -CR anomalies via χ annihilation, unless we invoke an enhancement mechanism of $\langle\sigma v\rangle$ at present [26, 27]. In other words, some $\Delta\Omega_\chi$ is necessitated in order to reconcile the best-fit $(m_\chi, \langle\sigma v\rangle)$ ’s with Eq. (1.2). Moreover, we observe that the bound of Eq. (5.4) (which turns out to be the most restrictive of all the others presented in Sec. 5.1) is violated in all cases. This violation, however, is softer in the case where χ ’s annihilate to $\mu^+\mu^-$. In this case, m_χ ’s and $\langle\sigma v\rangle$ ’s are pushed to larger values than those needed for $\chi\chi \rightarrow e^+e^-$. Best-fit $(m_\chi, \langle\sigma v\rangle)$ ’s consistent with all the available constraints are given in the next section.

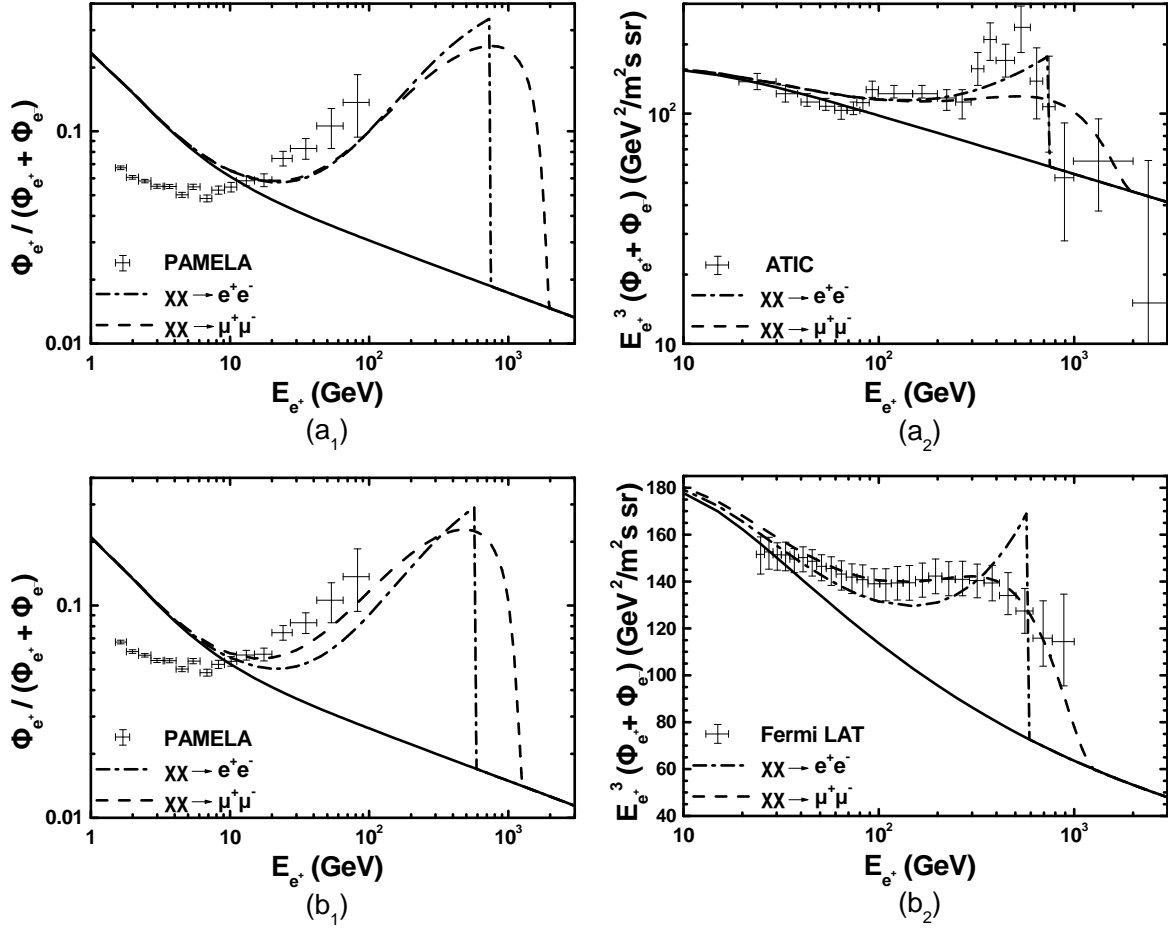


FIGURE 7: The e^+ -flux fraction (a₁ and b₁) and the total e^- and e^+ flux times $E_{e^+}^3$ (a₂ and b₂) as a function of E_{e^+} , with E_{e^+} being the e^+ energy. We use the best-fit points (m_χ , $\langle\sigma v\rangle$), indicated in Table 2, for the PAMELA and ATIC data (a₁ and a₂) or the PAMELA and Fermi-LAT data (b₁ and b₂), assuming χ annihilating into e^+e^- (dot-dashed lines) or $\mu^+\mu^-$ (dashed lines). The background fluxes are denoted by solid lines and are computed for $c_{e^-} = 0.6$ (a₁ and a₂) or $c_{e^-} = 0.7$ (b₁ and b₂). The data from PAMELA (a₁, b₁), ATIC (a₂) and Fermi-LAT (b₂) experiments are also shown (an additional uncertainty from the Fermi-LAT energy scale, which can shift all the points by 5% (up) to 10% (down) is not shown). Recall that we adopt the isothermal halo profile and the MED propagation model throughout.

FIGURE	ANNIHILATION MODE	$\chi^2 _{\min} /$ d.o.f	$m_\chi /$ TeV	$\langle\sigma v\rangle /$ 10^{-7} GeV^{-2}	$\langle\sigma v\rangle_{\max} /$ 10^{-7} GeV^{-2}	$\Omega_\chi h^2 _{\text{SC}} /$ 10^{-4}
7-(a ₁) and (a ₂)	$\chi\chi \rightarrow e^+e^-$	67/26	0.74	7.14	3.3	3.8
7-(a ₁) and (a ₂)	$\chi\chi \rightarrow \mu^+\mu^-$	76/26	2	28.6	26	0.97
7-(b ₁) and (b ₂)	$\chi\chi \rightarrow e^+e^-$	95/31	0.58	4.6	2.5	5.8
7-(b ₁) and (b ₂)	$\chi\chi \rightarrow \mu^+\mu^-$	24/31	1.28	19.5	16.5	1.4

TABLE 2: The best-fit points (m_χ , $\langle\sigma v\rangle$) for the PAMELA and ATIC data (used in Fig. 7-(a₁) and (a₂)) or the PAMELA and Fermi-LAT data (used in Fig. 7-(b₁) and (b₂)) for each annihilation channel of χ . Reported are also the corresponding $\chi^2|_{\min} / \text{d.o.f.}$, the maximal $\langle\sigma v\rangle$, $\langle\sigma v\rangle_{\max}$, allowed by Eq. (5.4) and the resulting $\Omega_\chi h^2$ in the SC, $\Omega_\chi h^2|_{\text{SC}}$.

5. RESTRICTIONS IN THE $m_\chi - \langle\sigma v\rangle$ PLANE

To systematize our approach, we need to delineate in the $m_\chi - \langle\sigma v\rangle$ plane the regions which are favored at 95% c.l. by the various experimental data on the e^\pm -CRs. In particular, we consider [55, 56] regions favored by PAMELA data only, PAMELA and ATIC data or PAMELA and Fermi LAT data. Since we have two independent parameters, m_χ and $\langle\sigma v\rangle$ these regions can be determined imposing the condition [56]

$$\chi^2 \lesssim \chi^2|_{\min} + 6 \quad \text{with} \quad \chi^2 = \begin{cases} \chi_1^2 & \text{for PAMELA,} \\ \chi_1^2 + \chi_2^2 & \text{for PAMELA and ATIC,} \\ \chi_1^2 + \chi_3^2 & \text{for PAMELA and Fermi LAT,} \end{cases} \quad (5.1)$$

where $\chi^2|_{\min}$ can be extracted numerically by minimization of χ^2 w.r.t m_χ and $\langle\sigma v\rangle$. On the other hand, the interpretation of the data on e^\pm -CRs in terms of χ annihilation can be viable if it can become consistent with a number of phenomenological constraints. In Sec. 5.1 we summarize these constraints and in Sec. 5.2 we examine if they can be reconciled with the regions favored by the data on e^\pm -CRs.

5.1 IMPOSED CONSTRAINTS

Though n_χ/s in Eq. (3.1) stays essentially unchanged for $\tau > \tau_f$, residual annihilations of χ 's occur up to the present with several cosmological consequences besides the possible interpretation of the data on e^\pm -CRs. Recently, tight upper bounds on $\langle\sigma v\rangle$'s have been reported and are summarized below together with the well-known unitarity constraint.

5.1.1 THE UNITARITY CONSTRAINT. Using partial-wave unitarity [23, 61] an upper limit, particularly relevant for $m_\chi > 2$ TeV, on $\langle\sigma v\rangle$ can be derived as a function of m_χ , i.e.,

$$\langle\sigma v\rangle \leq 8\pi \text{ GeV}^{-2} \left(\frac{m_\chi}{1 \text{ GeV}} \right)^{-2}. \quad (5.2)$$

5.1.2 THE BBN CONSTRAINT. During BBN, the χ annihilations inject an amount of energetic particles which is proportional to $\langle\sigma v\rangle$ and may strongly alter [33, 32] the abundances of the light elements. Ruining the successful predictions of the BBN can be avoided if we impose an upper bound on $\langle\sigma v\rangle$ which, however, depends on the identity of the products of the annihilation of χ 's. Taking into account the most up-to-date analysis of Ref. [32] we demand:

$$\langle\sigma v\rangle \leq 6 \cdot 10^{-7} \text{ GeV}^{-2} \frac{2m_\chi}{E_{\text{vis}}} \frac{m_\chi}{1 \text{ TeV}} \quad \text{where} \quad \frac{E_{\text{vis}}}{m_\chi} = \begin{cases} 2 & \text{for } \chi\chi \rightarrow e^+e^-, \\ 0.7 & \text{for } \chi\chi \rightarrow \mu^+\mu^-, \end{cases} \quad (5.3)$$

with E_{vis} being the total visible energy of the produced particles in the χ annihilation. We chose the annihilation modes above since they give the less restrictive bounds on $\langle\sigma v\rangle$ which can be reconciled [32] with the data on the e^\pm cosmic-ray fluxes.

5.1.3 THE CMB CONSTRAINT. The χ annihilations may have [34, 35] an impact on the ionization state of the baryonic gas at recombination and therefore on the CMB angular spectra. Consistency with the WMAP5 data [1] dictates [35] at 95% c.l. (see, also, Ref. [36]):

$$\langle\sigma v\rangle \leq \frac{3.1 \cdot 10^{-8} \text{ GeV}^{-2}}{f} \frac{m_\chi}{1 \text{ TeV}} \quad \text{where} \quad f \simeq \begin{cases} 0.7 & \text{for } \chi\chi \rightarrow e^+e^-, \\ 0.24 & \text{for } \chi\chi \rightarrow \mu^+\mu^-, \end{cases} \quad (5.4)$$

is the deposited power fraction which expresses the efficiency of the coupling between the annihilation products and the photon-baryon fluid at $z \sim 1000$. It is expected that forthcoming experiments will impose [35] even more stringent bounds on $\langle\sigma v\rangle$. Note, in passing, that the presence of q in the QKS does not affect recombination (which occurs at $\tau_{\text{rec}} \simeq -7$) since $\Omega_q(\tau_{\text{rec}})$ is safely suppressed provided that Eq. (2.28) is fulfilled.

5.1.4 CONSTRAINT FROM THE γ -COSMIC RAYS. The χ annihilation in the galactic center yields sizeable amount of γ -CRs, through the cascade decay of the annihilation products and/or brems-strahlung processes. Comparing the relevant γ -CR flux with the H.E.S.S observations [62] we can further restrict [31] $\langle\sigma v\rangle$ as a function of m_χ for the two chosen annihilation channels. However, this restriction significantly depends on the CDM halo profile. Adopting the cored isothermal CDM profile [58], which assures the less restrictive version of this constraint, we graphically extract the upper bound on $\langle\sigma v\rangle$ from the plots of Ref. [31]. To have a feeling of the straight of this constraint we can give some rough estimations:

$$\langle\sigma v\rangle \lesssim \begin{cases} 3 \cdot 10^{-6} \text{ GeV}^{-2} & \text{for } \chi\chi \rightarrow e^+e^-, \\ 4 \cdot 10^{-6} \text{ GeV}^{-2} & \text{for } \chi\chi \rightarrow \mu^+\mu^-. \end{cases} \quad (5.5)$$

Alternatively this constraint can be evaded for every CDM profile, by allowing the χ -annihilation products to be long lived, as pointed out in Ref. [56].

Complementary constraints on the χ annihilation can be imposed comparing the findings of EGRET satellite [64] with the diffuse (secondary) γ -CR fluxes, which would be produced [63] by inverse Compton scatterings on interstellar photons of the energetic e^\pm generated by the χ annihilation in the galactic halo. However, these bounds are expected [63] to be weaker than the ones imposed by the high energy γ -CRs mentioned in Sec. 5.1.4 and are not included in our analysis. Similar arguments are [65] also valid for the neutrinos generated from the χ annihilation in the galactic center, though the dependence on the CDM profile is weaker.

5.2 RESULTS

Fixing the parameters related to the LRS [QKS] to some representative values – consistent with Sec. 2.2.2 [Sec. 2.3.2] –, we can display in the $m_\chi - \langle\sigma v\rangle$ plane, as in Fig. 8, the restrictions from all the requirements above together with the preferred areas by the various experimental data. Fig. 8-(a₁) and (a₂) are devoted to the LRS whereas Fig. 8-(b₁), (b₂), (c₁) and (c₂) analyze the QKS. In Fig. 8-(a₁), (b₁) and (c₁) [Fig. 8-(a₂), (b₂) and (c₂)] we assume that χ annihilates into e^+e^- [$\mu^+\mu^-$].

For the LRS, we confine ourselves to some combinations of parameters which assure a sufficient coexistence of non-TP and TP, since the non-TP alone is obviously – see Eq. (3.7) – $\langle\sigma v\rangle$ independent and therefore can not be properly depicted in the $m_\chi - \langle\sigma v\rangle$ plane. We take $(c_{\chi\phi}, T_{\text{RH}}) = (2 \cdot 10^{-6}, 0.1 \text{ GeV})$ and $(c_{\chi\phi}, T_{\text{RH}}) = (1, 1 \text{ GeV})$ [$(c_{\chi\phi}, T_{\text{RH}}) = (10^{-6}, 0.1 \text{ GeV})$ and $(c_{\chi\phi}, T_{\text{RH}}) = (1, 0.5 \text{ GeV})$] in Fig. 8-(a₁) [Fig. 8-(a₂)]. For the QKS, we set throughout $a = 0.5$, $T_1 = 10^9 \text{ GeV}$. We also take (i) $b = 0$ and $\bar{H}_1 = 6.3 \cdot 10^{53}$, $2 \cdot 10^{53}$ or $6.2 \cdot 10^{52}$ resulting to $\Omega_q^{\text{BBN}} = 0.01, 0.001$ or 0.0001 respectively in Fig. 8-(b₁) and (b₂); (ii) $\bar{H}_1 = 6.3 \cdot 10^{53}$ and $b = 0.15$ [$\bar{H}_1 = 6.2 \cdot 10^{52}$ and $b = 0.32$] resulting to $\Omega_q^{\text{BBN}} = 0.068$ or [$\Omega_q^{\text{BBN}} = 0.065$] in Fig. 8-(c₁); (iii) $\bar{H}_1 = 6.3 \cdot 10^{53}$ and $b = 0.32$ [$\bar{H}_1 = 2 \cdot 10^{53}$ and $b = 0.2$] yielding $\Omega_q^{\text{BBN}} = 0.19$ or [$\Omega_q^{\text{BBN}} = 0.21$] in Fig. 8-(c₂). Note that in Fig. 8-(b₁) and (b₂) we present for the sake of comparison results even for $b = 0$, although the tracking behavior of the QKS is not attained in this case – see Sec. 2.3.4.

In the plots of Fig. 8, the light gray shaded regions are confronted with Eq. (1.2). The gray dashed [dotted] lines correspond to Eq. (1.2b) [Eq. (1.2a)], whereas the gray solid lines are obtained by fixing $\Omega_\chi h^2$ to its central value in Eq. (1.2). We observe that $\Omega_\chi h^2$ decreases as $\langle\sigma v\rangle$ increases. This is due to the fact that $\Omega_\chi h^2 \propto 1/\langle\sigma v\rangle$ as can be deduced from Eq. (3.1) and Eq. (3.8) [Eq. (3.9)] for the LRS [QKS]. For the LRS, as it is clear from these plots, there is a minor slice of the allowed region with $m_\chi < 0.35$ TeV [$m_\chi < 0.8$ TeV] for $T_{\text{RH}} = 0.1$ GeV and $c_{\chi\phi} = 2 \cdot 10^{-6}$ [$c_{\chi\phi} = 10^{-6}$] where non-TP is strengthened and our results are almost $\langle\sigma v\rangle$ independent. For the QKS, we also observe that for τ_{F} far away from τ_{ext} the allowed by Eq. (1.2) for $b \neq 0$ region reaches the one for $b = 0$ – with fixed \bar{H}_1 . However, when τ_{F} reaches τ_{ext} , $\Omega_\chi h^2$ decreases (as we explain in Sec. 3.2) and so, the required, for obtaining $\Omega_\chi h^2$ in the range of Eq. (1.2), $\langle\sigma v\rangle$ decreases too. As a consequence, although the allowed by Eq. (1.2) area in Fig. 8-(c₁) [Fig. 8-(c₂)] for $\bar{H}_1 = 6.3 \cdot 10^{53}$ approaches the corresponding area in Fig. 8-(b₁) [Fig. 8-(b₂)] with the same \bar{H}_1 and violates the bounds of Eqs. (5.3) and (5.4) for low m_χ 's, they become compatible with the latter constraints for larger m_χ 's. On the other hand, we observe that there is no such a transition region in the light gray area of Fig. 8-(c₂). This is, because for $0.1 \leq m_\chi/\text{TeV} \leq 3$ we get $31.8 \leq -\tau_{\text{F}} \leq 35.1$ whereas the closest to τ_{F} 's, τ_{ext} is $\tau_{\text{ext}} = -35.4$ which remains constantly lower than τ_{F} . Therefore, no reduction of $\Delta\Omega_\chi$ occurs for the m_χ 's used in Fig. 8-(c₂).

In Fig. 8 we also delineate the regions preferred at 95% c.l. by PAMELA data (black and red sparse hatched areas), PAMELA and ATIC data (dense black hatched areas) and PAMELA and Fermi-LAT data (dense red hatched areas), by imposing the condition of Eq. (5.1). In the black [red] hatched areas the background fluxes are normalized setting $c_{e^-} = 0.6$ [$c_{e^-} = 0.7$] in Eq. (4.6). Evidently, the PAMELA data do not prefer any m_χ since it does not show any peak structure. On the other hand, the regions derived by the joint analysis of two data-sets are much more limited – c.f. Ref. [31, 36, 56]. We consider the latter approach as more reliable, since even when we fit only the PAMELA data, the data points with low E_{e^+} from ATIC/Fermi LAT are involved, in order to normalize [56] the background fluxes.

In Fig. 8 drawn is also the upper bound from Eqs. (5.2), (5.3) and (5.4), denoted by a black dotted, solid and dashed line respectively and this from the constraint of Sec. 5.1.4, depicted by a dot-dashed line. Obviously acceptable are the regions mainly below the dashed curves, since the bound of Eq. (5.4) is the most restrictive from the others. These regions are just marginally consistent with the explanation of the experimental anomalies via the annihilation mode $\chi\chi \rightarrow e^+e^-$ as can be deduced from Fig. 8-(a₁), (b₁) and (c₁). Indeed, in this case, the regions preferred at 95% c.l. from both combinations of the experimental data are entirely excluded from the bounds of Eqs. (5.3) and (5.4) – c.f. Ref. [32, 36]. On the other hand, the picture is certainly ameliorated in the case with $\chi\chi \rightarrow \mu^+\mu^-$, which prefers [23, 32, 56, 65] higher m_χ 's and $\langle\sigma v\rangle$'s – see Fig. 8-(a₂), (b₂) and (c₂). There, we observe that (i) portions of the favored regions at 95% c.l. by the PAMELA and ATIC or Fermi-LAT data lie very close or even lower than the limits of Eq. (5.3) and/or (5.4) and (ii) the bound of Eq. (5.2) cuts out some minor slices of the parameter space for large m_χ 's.

Needless to say that the bounds inferred by Eqs. (5.3) and (5.4), Sec. 5.1.4 and the areas which are favored by the various experimental data depends on the χ -annihilation mode but are independent of the scenario considered. On the other hand, the areas allowed by Eq. (1.2) and Eq. (5.2) are independent (in our approach) of the χ -annihilation mode. The areas allowed by Eq. (1.2) depend on the parameters of the LRS ($c_{\chi\phi}$ and T_{RH}) or the QKS (a , b , \bar{H}_1 and T_1).

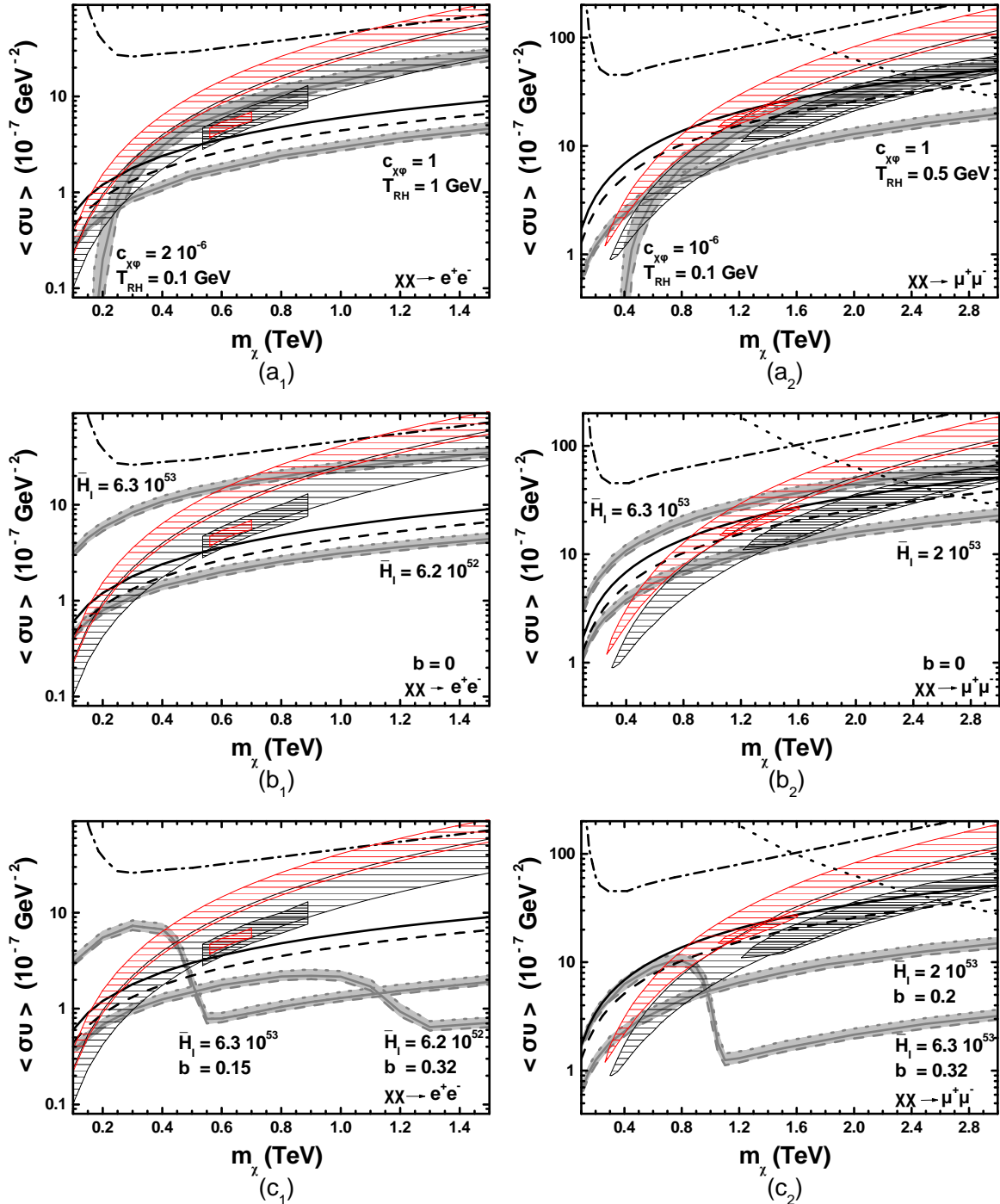


FIGURE 8: Restrictions in the $m_\chi - \langle\sigma v\rangle$ plane for the LRS (a₁, a₂) [QKS (b₁, b₂, c₁, c₂) taking $a = 0.5$, $T_1 = 10^9$ GeV] with various $c_{\chi\phi}$'s and T_{RH} 's [b 's and \bar{H}_1 's], indicated in the graphs, and χ 's annihilating into e^+e^- (a₁, b₁, c₁) or $\mu^+\mu^-$ (a₂, b₂, c₂). The light gray shaded areas are allowed by Eq. (1.2), the sparse black [red] hatched areas are preferred at 95% c.l. by the PAMELA data for $c_{e^-} = 0.6$ [$c_{e^-} = 0.7$] and the dense black [red] hatched areas are preferred at 95% c.l. by the PAMELA and ATIC [PAMELA and Fermi-LAT] data. Regions above the black solid, dashed, dotted and dot-dashed lines are ruled out by the upper bounds on $\langle\sigma v\rangle$ from Eq. (5.3), (5.4), (5.2) and Sec. 5.1.4 correspondingly. The conventions adopted for the residual lines are also shown.

- $\Omega_\chi h^2 = 0.097$
- $\Omega_\chi h^2 = 0.11$
- $\Omega_\chi h^2 = 0.12$

As can be concluded from most of the plots of Fig. 8, a simultaneous interpretation of the e^\pm -CR anomalies consistently with the requirements of Sec. 5.1 can be achieved in the regions where the gray shaded areas overlap the lined ones below the dashed lines. To highlight this intriguing conclusion of this paper, it would be interesting to find the best-fit $(m_\chi, \langle\sigma v\rangle)$ (for the various combined data-sets) which fulfill all the restrictions imposed in Sec. 5.1. Our results are arranged in Table 3. The listed $(m_\chi, \langle\sigma v\rangle)$'s saturate the bound of Eq. (5.4) which turns out to be essentially the most stringent of the others – see Fig. 8. We observe that $m_\chi \sim 0.1$ TeV and $\langle\sigma v\rangle \sim 10^{-7}$ GeV $^{-2}$ [$m_\chi \sim 1$ TeV and $\langle\sigma v\rangle \sim 10^{-6}$ GeV $^{-2}$] for χ 's annihilating to e^+e^- [$\mu^+\mu^-$]. From the exposed in Table 3 $\chi^2 - \chi^2|_{\min}$'s, we deduce that all the requirements are met in a portion of the area favored at 99% c.l. [68% c.l.] by the PAMELA and Fermi-LAT [ATIC] data for $\chi\chi \rightarrow \mu^+\mu^-$. As regards the quality of the fits, from Tables 2 and 3, we can infer that the $\mu^+\mu^-$ channel gives better fit to the PAMELA and Fermi-LAT data ($\chi^2/\text{d.o.f} = 33/31$) than to the PAMELA and ATIC data ($\chi^2/\text{d.o.f} = 77/26$).

From Table 3 we can also appreciate the importance of the non-SC in boosting $\Omega_\chi h^2$ to an acceptable level. Indeed, in this Table we display $\Omega_\chi h^2|_{\text{SC}}$ for every allowed best-fit $(m_\chi, \langle\sigma v\rangle)$. We observe that it lies much lower than the range of Eq. (1.2) in all cases, i.e., it is insufficient to account for the present CDM abundance in the universe. However, an appropriate adjustment (shown also in Table 3) of the parameters $c_{\chi\phi}$ and T_{RH} [b and \bar{H}_1 (with fixed $a = 0.5$ and $T_1 = 10^9$ GeV)] for the LRS [QKS] – consistently with the restrictions of Sec. 2.2.2 [Sec. 2.3.2] – elevates adequately $\Omega_\chi h^2$ which can acquire the central experimental value in Eq. (1.2) for every best-fit point. In Table 3 we also expose the type of χ production for the LRS and the transition temperature to the RD era for the QKS. We remark that since the $\langle\sigma v\rangle$'s required for χ 's annihilating to e^+e^- are lower than those required for the $\mu^+\mu^-$ channel, the non-TP dominates even for $T_{\text{RH}} = 0.1$ GeV. Note that $T_{\text{KR}} \leq 0.04$ GeV and the tracking behavior fails for $b = 0$ in the case of the QKS.

6. CONCLUSIONS

We presented two non-standard cosmological scenaria which can increase the relic abundance of a WIMP χ , $\Omega_\chi h^2$, w.r.t its value in the SC due to the generation of a background energy density steeper than this of RD era. This increase is quantified by $\Delta\Omega_\chi$ defined in Eq. (3.10). According to the first scenario, termed LRS, a scalar field ϕ decays, reheating the universe to a reheating temperature lower than the freeze-out temperature of the WIMPs. According to the second scenario, termed QKS, a scalar field, q , rolls down its inverse power-low potential with a Hubble-induced mass term. In both cases our approach was both (i) purely numerical, integrating the relevant system of the differential equations (ii) semi-analytical, producing approximate relations for the evolution of the various energy densities of the cosmological background and the χ -number density. We consider that the exposed semi-analytical findings – although do not provide quite accurate results in all cases – facilitate the understanding of the cosmological dynamics.

As regards the LRS, we recalled the dynamics of reheating and showed that $\Delta\Omega_\chi$ is affected by the two basic types of χ production which can be discriminated, depending whether non-TP dominates or equally contributes with the TP. The first type is activated for very low T_{RH} , low N_χ and is more or less independent of $\langle\sigma v\rangle$, whereas the latter case requires larger T_{RH} 's and N_χ 's and depends on $\langle\sigma v\rangle$. In this last case, we remarked that a short period of χ reannihilation can emerge.

FITS TO PAMELA AND ATIC DATA						
	$\chi\chi \rightarrow e^+e^-$			$\chi\chi \rightarrow \mu^+\mu^-$		
m_χ (TeV)	0.47			2		
$\langle\sigma v\rangle$ (GeV^{-2})	$2.1 \cdot 10^{-7}$			$2.6 \cdot 10^{-6}$		
$\chi^2 - \chi^2_{\min}$	15.8			1		
$\Omega_\chi h^2 _{\text{SC}}$	0.0012			0.0001		
COMBINATIONS OF PARAMETERS YIELDING $\Omega_\chi h^2 = 0.11$ IN THE LRS						
T_{RH} (GeV)	0.001	0.1	0.67	0.001	0.1	0.27
$c_{\chi\phi}$	$8 \cdot 10^{-5}$	$1.2 \cdot 10^{-6}$	1	$1.9 \cdot 10^{-5}$	$9 \cdot 10^{-7}$	1
χ -PRODUCTION	NON-TP		NON-TP + TP	NON-TP	NON-TP + TP	
COMBINATIONS OF PARAMETERS YIELDING $\Omega_\chi h^2 = 0.11$ IN THE QKS FOR $a = 0.5$ AND $T_I = 10^9$ GeV						
b	0	0.2	0.32	0	0.08	
$\bar{H}_I/10^{53}$	0.88	1.35	1	3.5	3.7	
T_{KR} (GeV)	0.06	0.03	0.097	0.017	0.005	
FITS TO PAMELA AND FERMI-LAT DATA						
	$\chi\chi \rightarrow e^+e^-$			$\chi\chi \rightarrow \mu^+\mu^-$		
m_χ (TeV)	0.258			1.12		
$\langle\sigma v\rangle$ (GeV^{-2})	$1.14 \cdot 10^{-7}$			$1.44 \cdot 10^{-6}$		
$\chi^2 - \chi^2_{\min}$	177			9		
$\Omega_\chi h^2 _{\text{SC}}$	0.0022			0.00019		
COMBINATIONS OF PARAMETERS YIELDING $\Omega_\chi h^2 = 0.11$ IN THE LRS						
T_{RH} (GeV)	0.001	0.1	0.67	0.001	0.1	0.27
$c_{\chi\phi}$	$1.4 \cdot 10^{-4}$	$2.2 \cdot 10^{-6}$	1	$3.3 \cdot 10^{-5}$	$1.4 \cdot 10^{-6}$	1
χ -PRODUCTION	NON-TP		NON-TP + TP	NON-TP	NON-TP + TP	
COMBINATIONS OF PARAMETERS YIELDING $\Omega_\chi h^2 = 0.11$ IN THE QKS FOR $a = 0.5$ AND $T_I = 10^9$ GeV						
b	0	0.2	0.32	0	0.08	0.18
$\bar{H}_I/10^{53}$	0.76	1.2	0.96	3.1	3.4	4.7
T_{KR} (GeV)	0.07	0.03	0.04	0.019	0.005	0.009

TABLE 3: Best-fit (m_χ , $\langle\sigma v\rangle$)'s for the combination of the PAMELA and ATIC or Fermi-LAT data and the various annihilation channels, consistently with all the imposed constraints. Shown is also the resulting $\chi^2 - \chi^2_{\min}$ and $\Omega_\chi h^2$ in the SC, $\Omega_\chi h^2|_{\text{SC}}$, several combinations of (b , \bar{H}_I)'s [$(T_{\text{RH}}, c_{\chi\phi})$'s] leading to $\Omega_\chi h^2 \simeq 0.11$ and the corresponding T_{KR} 's [types of χ production] within the QKS [LRS].

As regards the QKS, we verified that the included Hubble-induced mass term ensures the presence of a KD period, which is characterized by an oscillating evolution of q , and allows the quintessential energy density to join in time a tracker behavior, alleviating, thereby, the coincidence problem. Observational data originating from BBN, the present acceleration of the universe, the inflationary scale and the DE density parameter can be also met in a sizable fraction of the parameter space of the model. $\Delta\Omega_\chi$ crucially depends on the hierarchy between the freeze-out temperature and the temperature where the evolution of q develops extrema.

Assuming that the WIMP annihilates primarily to e^+e^- or $\mu^+\mu^-$ we calculated the induced flux of e^\pm -CRs and fit the current data of PAMELA, ATIC and Fermi LAT without invoking any ad-hoc boost factor. For simplicity, we did not include in our fits older experimental results, such as from PPB-BETS [66], or more uncertain ones, such as from H.E.S.S [67]. Taking into account constraints originating from BBN and CMB, we concluded that (i) large parts of the regions favored by PAMELA for both annihilation modes are ruled out; (ii) regions favored by PAMELA and ATIC or Fermi LAT for $\chi\chi \rightarrow e^+e^-$ are excluded; (iii) only a part of the region favored by PAMELA and ATIC data at 95% c.l. for $\chi\chi \rightarrow \mu^+\mu^-$ can be acceptable. For the latter annihilation channel we achieved our best fits to PAMELA and Fermi-LAT data with $m_\chi \sim 1$ TeV and $\langle\sigma v\rangle \sim 10^{-6}$ GeV $^{-2}$ which are consistent with restrictions above and belong within the region individuated by these data-sets at 99% c.l. These m_χ 's and $\langle\sigma v\rangle$'s can yield the right amount of $\Omega_\chi h^2$ (entailed by the CDM considerations) by adjusting the parameters of the QKS or LRS. In both scenaria the required transition temperature to the conventional RD era turns out to be lower than about 0.7 GeV. In the case of the LRS an appreciable contribution of the non-TP is also necessitated.

As for the prediction of any CDM signal, there are three sources of uncertainty in our investigation: the CDM distribution, the propagation of its annihilation products and the role of astrophysical backgrounds. In our analysis we used (i) the isothermal halo profile, to avoid troubles [31] with observations on γ -CRs; (ii) the MED propagation model, which provides the best fits to the combinations of the various data-sets [55] and (iii) commonly assumed background e^+ and e^- fluxes [50] normalized with the ATIC or Fermi-LAT data. The uncertainties above in conjunction with the very stringent constraints from BBN and CMB may jeopardize the interpretation of the PAMELA and ATIC or Fermi-LAT anomalies through the χ annihilation. Therefore, the proposed scenaria can be probed in the near future, if a better understanding of the astrophysical uncertainties becomes available and/or more accurate experimental data are released.

Our proposal could be supplemented by the construction of a particle model (see, e.g., Ref. [55, 68]) with the appropriate couplings so that χ annihilates into $\mu^+\mu^-$ with the desired $\langle\sigma v\rangle$'s derived self-consistently with the (s)particle spectrum. In a such case several phenomenological implications could be examined as in Ref. [15]. Let us finally mention that another class of non-standard cosmological scenaria [8, 23, 49, 69, 70] can be generated considering modifications to the Friedmann equations due to corrections to the Einstein gravity. Constraining these possibilities through the experimental results on e^\pm -CRs would be another interesting issue.

ACKNOWLEDGMENTS

This research was funded by the FP6 Marie Curie Excellence Grant MEXT-CT-2004-014297. The author would like to thank A.B. Lahanas for valuable discussions and N. Vlachos for providing helpful software.

REFERENCES

- [1] E. KOMATSU *et al.* [WMAP COLLABORATION], *Astrophys. J. Suppl.* **180**, 330 (2009) [arXiv:0803.0547]
<http://lambda.gsfc.nasa.gov/product/map/dr2/parameters.cfm>.
- [2] *For a review from the viewpoint of particle physics, see*
 A.B. LAHANAS, N.E. MAVROMATOS AND D.V. NANOPOULOS, *Int. J. Mod. Phys. D* **12**, 1529 (2003) [hep-ph/0308251].
- [3] K. MATCHEV, hep-ph/0402088; E.A. BALTZ, astro-ph/0412170; G. LAZARIDES, hep-ph/0601016;
 M. TAOSO, G. BERTONE AND A. MASIERO, *J. Cosmol. Astropart. Phys.* **03**, 022 (2008) [arXiv:0711.4996].
- [4] G. JUNGMAN, M. KAMIONKOWSKI AND K. GRIEST, *Phys. Rep.* **267**, 195 (1996) [hep-ph/9506380].
- [5] G. SERVANT AND T.M.P. TAIT, *Nucl. Phys.* **B650**, 391 (2003) [hep-ph/0206071];
 H.C. CHENG *et al.*, *Phys. Rev. Lett.* **89**, 211301 (2002) [hep-ph/0207125];
 K. AGASHE AND G. SERVANT, *Phys. Rev. Lett.* **93**, 231805 (2004) [hep-ph/0403143];
 J.A.R. CEMBRANOS *et al.*, *Phys. Rev. Lett.* **90**, 241301 (2003) [hep-ph/0302041].
- [6] J. McDONALD, *Phys. Rev. Lett.* **88**, 091304 (2002) [hep-ph/0106249];
 M. CIRELLI, N. FORNENGO AND A. STRUMIA, *Nucl. Phys.* **B753**, 178 (2006) [hep-ph/0512090];
 T. ASAKA, K. ISHIWATA AND T. MOROI, *Phys. Rev. D* **73**, 051301 (2006) [hep-ph/0512118];
 D.G. CERDEÑO, C. MUÑOZ AND O. SETO, *Phys. Rev. D* **79**, 023510 (2009) [arXiv:0807.3029];
 F. DEPPISCH AND A. PILAFTSIS, *J. High Energy Phys.* **10**, 080 (2008) [arXiv:0808.0490].
- [7] H. GOLDBERG, *Phys. Rev. Lett.* **50**, 1419 (1983);
 J.R. ELLIS *et al.*, *Nucl. Phys.* **B238**, 453 (1984).
- [8] M. KAMIONKOWSKI AND M.S. TURNER, *Phys. Rev. D* **42**, 3310 (1990);
 C. PALLIS, “*The Identification of Dark Matter*”, pp. 602-608 [hep-ph/0610433].
- [9] T. MOROI AND L. RANDALL, *Nucl. Phys.* **B570**, 455 (2000) [hep-ph/9906527];
 R. ALLAHVERDI AND M. DREES, *Phys. Rev. Lett.* **89**, 091302 (2002) [hep-ph/0203118].
- [10] J. McDONALD, *Phys. Rev. D* **43**, 1063 (1991);
 T. NAGANO AND M. YAMAGUCHI, *Phys. Lett. B* **438**, 267 (1998) [hep-ph/9805204];
 G.F. GIUDICE, E.W. KOLB AND A. RIOTTO, *Phys. Rev. D* **64**, 023508 (2001) [hep-ph/0005123];
 N. FORNENGO, A. RIOTTO AND S. SCOPEL, *Phys. Rev. D* **67**, 023514 (2003) [hep-ph/0208072].
- [11] C. PALLIS, *Astropart. Phys.* **21**, 689 (2004) [hep-ph/0402033];
 C. PALLIS, *Nucl. Phys.* **B751**, 129 (2006) [hep-ph/0510234].
- [12] G.B. GELMINI AND P. GONDOLO, *Phys. Rev. D* **74**, 023510 (2006) [hep-ph/0602230];
 G. GELMINI, P. GONDOLO, A. SOLDATENKO AND C.E. YAGUNA, *Phys. Rev. D* **74**, 083514 (2006) [hep-ph/0605016].
- [13] M. NAGAI AND K. NAKAYAMA, *Phys. Rev. D* **78**, 063540 (2008) [arXiv:0807.1634];
 B. DUTTA, L. LEBLOND AND K. SINHA, *Phys. Rev. D* **80**, 035014 (2009) [arXiv:0904.3773];
 J. McDONALD, arXiv:0904.0969.
- [14] P. SALATI, *Phys. Lett. B* **571**, 121 (2003) [astro-ph/0207396].
- [15] S. PROFUMO AND P. ULLIO, *J. Cosmol. Astropart. Phys.* **11**, 006 (2003) [hep-ph/0309220];
 D.J.H. CHUNG *et al.*, *J. High Energy Phys.* **10**, 016 (2007) [arXiv:0706.2375].
- [16] C. PALLIS, *J. Cosmol. Astropart. Phys.* **10**, 015 (2005) [hep-ph/0503080];
 M.E. GÓMEZ *et al.*, *J. Cosmol. Astropart. Phys.* **01**, 027 (2009) [arXiv:0809.1859];
 M.E. GÓMEZ *et al.*, *AIP Conf. Proc.* **1115**, 157 (2009) [arXiv:0809.1982].
- [17] B. SPOKOINY, *Phys. Lett. B* **315**, 40 (1993) [gr-qc/9306008];
 M. JOYCE, *Phys. Rev. D* **55**, 1875 (1997) [hep-ph/9606223];
 P.G. FERREIRA AND M. JOYCE, *Phys. Rev. D* **58**, 023503 (1998) [astro-ph/9711102].

- [18] P.J. PEEBLES AND A. VILENKIN, *Phys. Rev. D* **59**, 063505 (1999) [astro-ph/9810509];
M. YAHIRO *et al.*, *Phys. Rev. D* **65**, 063502 (2002) [astro-ph/0106349];
K. DIMOPOULOS AND J.W. VALLE, *Astropart. Phys.* **18**, 287 (2002) [astro-ph/0111417];
K. DIMOPOULOS, *Phys. Rev. D* **68**, 123506 (2003) [astro-ph/0212264];
I.P. NEUPANE, *Class. Quant. Grav.* **25**, 125013 (2008) [arXiv:0706.2654];
M. BASTERO-GIL, A. BERERA, B.M. JACKSON AND A. TAYLOR, *Phys. Lett. B* **678**, 157 (2009) [arXiv:0905.2937].
- [19] D.J.H. CHUNG, L.L. EVERETT AND K.T. MATCHEV, *Phys. Rev. D* **76**, 103530 (2007) [arXiv:0704.3285];
G. BARENBOIM AND J.D. LYKKEN, *J. High Energy Phys.* **12**, 005 (2006) [hep-ph/0608265];
G. BARENBOIM AND J.D. LYKKEN, *J. High Energy Phys.* **10**, 032 (2007) [arXiv:0707.3999].
- [20] A. MASIERO, M. PIETRONI AND F. ROSATI, *Phys. Rev. D* **61**, 023504 (2000) [hep-ph/9905346];
F. ROSATI, *Phys. Lett. B* **570**, 5 (2003) [hep-ph/0302159].
- [21] S. LOLA, C. PALLIS AND E. TZELATI, arXiv:0907.2941.
- [22] P. BINETRUI, *Int. J. Theor. Phys.* **39**, 1859 (2000) [hep-ph/0005037];
E.J. COPELAND *et al.*, *Int. J. Mod. Phys. D* **15**, 1936 (2006) [hep-th/0603057].
- [23] A.A.E. ZANT, S. KHALIL AND H. OKADA, arXiv:0903.5083;
W.L. GUO AND X. ZHANG, *Phys. Rev. D* **79**, 115023 (2009) [arXiv:0904.2451].
- [24] O. ADRIANI *et al.* [PAMELA COLLABORATION], *Nature* **458**, 607 (2009) [arXiv:0810.4995].
- [25] J. CHANG *et al.* [ATIC COLLABORATION], *Nature* **456**, 362 (2008).
- [26] M. IBE, H. MURAYAMA AND T.T. YANAGIDA, *Phys. Rev. D* **79**, 095009 (2009) [arXiv:0812.0072];
W.L. GUO AND Y.L. WU, *Phys. Rev. D* **79**, 055012 (2009) [arXiv:0901.1450].
- [27] J. HISANO, S. MATSUMOTO, M. M. NOJIRI AND O. SAITO, *Phys. Rev. D* **71**, 063528 (2005) [hep-ph/0412403];
N. ARKANI-HAMED *et al.*, *Phys. Rev. D* **79**, 015014 (2009) [arXiv:0810.0713];
M. LATTANZI AND J.I. SILK, *Phys. Rev. D* **79**, 083523 (2009) [arXiv:0812.0360];
J.D. MARCH-RUSSELL AND S.M. WEST, *Phys. Lett. B* **676**, 133 (2009) [arXiv:0812.0559];
X.G. HE, arXiv:0908.2908.
- [28] D. HOOPER, *et al.*, *J. Cosmol. Astropart. Phys.* **01**, 025 (2009) [arXiv:0810.1527];
H. YUKSEL, M. D. KISTLER AND T. STANEV, *Phys. Rev. Lett.* **103**, 051101 (2009) [arXiv:0810.2784].
- [29] S.W. BARWICK *et al.* [HEAT COLLABORATION], *Astrophys. J.* **482**, L191 (1997) [astro-ph/9703192];
M. AGUILAR *et al.* [AMS-01 COLLABORATION], *Phys. Lett. B* **646**, 145 (2007) [astro-ph/0703154].
- [30] A.A. ABDO *et al.* [THE FERMI-LAT COLLABORATION], *Phys. Rev. Lett.* **102**, 181101 (2009) [arXiv:0905.0025].
- [31] G. BERTONE, M. CIRELLI, A. STRUMIA AND M. TAOSO, *J. Cosmol. Astropart. Phys.* **03**, 009 (2009) [arXiv:0811.3744].
- [32] J. HISANO *et al.*, *Phys. Rev. D* **79**, 083522 (2009) [arXiv:0901.3582].
- [33] M. H. RENO AND D. SECKEL, *Phys. Rev. D* **37**, 3441 (1988);
J.A. FRIEMAN, E.W. KOLB AND M.S. TURNER, *Phys. Rev. D* **41**, 3080 (1990);
K. JEDAMZIK, *Phys. Rev. D* **70**, 083510 (2004) [astro-ph/0405583].
- [34] N. PADMANABHAN AND D.P. FINKBEINER, *Phys. Rev. D* **72**, 023508 (2005) [astro-ph/0503486];
L. ZHANG, X.L. CHEN, Y.A. LEI AND Z.G. SI, *Phys. Rev. D* **74**, 103519 (2006) [astro-ph/0603425].
- [35] S. GALLI, F. IOCCO, G. BERTONE AND A. MELCHIORRI, *Phys. Rev. D* **80**, 023505 (2009) [arXiv:0905.0003];
T.R. SLATYER, N. PADMANABHAN AND D.P. FINKBEINER, *Phys. Rev. D* **80**, 043526 (2009) [arXiv:0906.1197].
- [36] G. HUETSI, A. HEKTOR AND M. RAIDAL, arXiv:0906.4550;
M. CIRELLI, F. IOCCO AND P. PANCI, arXiv:0907.0719;
T. KANZAKI, M. KAWASAKI AND K. NAKAYAMA, arXiv:0907.3985.
- [37] M. DINE, L. RANDALL AND S.D. THOMAS, *Phys. Rev. Lett.* **75**, 398 (1995) [hep-ph/9503303];
D.J.H. CHUNG, L.L. EVERETT AND A. RIOTTO, *Phys. Lett. B* **556**, 61 (2003) [hep-ph/0210427].

- [38] S.D.H. HSU AND B. MURRAY, *Phys. Lett. B* **595**, 16 (2004) [astro-ph/0402541];
D.J. LIU AND X.Z. LI, *Phys. Lett. B* **611**, 8 (2005) [astro-ph/0501596];
W.Z. LIU AND D.J. LIU, arXiv:0803.4039.
- [39] P.J. STEINHARDT, L. WANG AND I. ZLATEV, *Phys. Rev. Lett.* **82**, 896 (1999) [astro-ph/9807002];
ibid., *Phys. Rev. D* **59**, 123504 (1999) [astro-ph/9812313].
- [40] B. RATRA AND P.J.E. PEEBLES, *Phys. Rev. D* **37**, 3406 (1988);
A.R. LIDDLE AND R.J. SCHERRER, *Phys. Rev. D* **59**, 023509 (1999) [astro-ph/9809272];
J.P. UZAN, *Phys. Rev. D* **59**, 123510 (1999) [gr-qc/9903004].
- [41] G. BÉLANGER *et al.*, *Comput. Phys. Commun.* **149**, 103 (2002) [hep-ph/0112278];
P. GONDOLO *et al.*, *J. Cosmol. Astropart. Phys.* **07**, 008 (2004) [astro-ph/0406204].
- [42] R.H. CYBURT *et al.*, *Astropart. Phys.* **23**, 313 (2005) [astro-ph/0408033].
- [43] S. DAVIDSON AND S. SARKAR, *J. High Energy Phys.* **11**, 012 (2000) [hep-ph/0009078].
- [44] M. ENDO *et al.*, *Phys. Rev. Lett.* **96**, 211301 (2006) [hep-ph/0602061];
S. NAKAMURA AND M. YAMAGUCHI, *Phys. Lett. B* **638**, 389 (2006) [hep-ph/0602081].
- [45] M. TEGMARK *et al.*, *Phys. Rev. D* **69**, 103501 (2004) [astro-ph/0310723];
A.G. RIESS *et al.*, *Astrophys. J.* **607**, 665 (2004) [astro-ph/0402512].
- [46] P. BINETRUY, *Phys. Rev. D* **60**, 063502 (1999) [hep-ph/9810553];
P. BINETRUY, *Supersymmetry*, Oxford University Press (2006).
- [47] C. BACCIGALUPI *et al.*, *Phys. Rev. D* **65**, 063520 (2002) [astro-ph/0109097].
- [48] G. LAZARIDES, R.K. SCHAEFER, AND Q. SHAFI, *Phys. Rev. D* **56**, 1324 (1997) [hep-ph/9608256].
- [49] R. CATENA *et al.*, *Phys. Rev. D* **70**, 063519 (2004) [astro-ph/0403614];
R. CATENA *et al.*, *J. High Energy Phys.* **10**, 003 (2008) [arXiv:0712.3173].
- [50] E.A. BALTZ AND J. EDSJO, *Phys. Rev. D* **59**, 023511 (1999) [astro-ph/9808243].
- [51] J. HISANO, S. MATSUMOTO, O. SAITO AND M. SENAMI, *Phys. Rev. D* **73**, 055004 (2006) [hep-ph/0511118];
T. DELAHAYE *et al.*, *Phys. Rev. D* **77**, 063527 (2008) [arXiv:0712.2312].
- [52] M. CIRELLI, R. FRANCESCHINI AND A. STRUMIA, *Nucl. Phys.* **B800**, 204 (2008) [arXiv:0802.3378].
- [53] O. ADRIANI *et al.* [PAMELA COLLABORATION], *Phys. Rev. D* **102**, 051101 (2009) [arXiv:0810.4994].
- [54] P. GRAJEK, G. KANE, D. PHALEN, A. PIERCE AND S. WATSON, *Phys. Rev. D* **79**, 043506 (2009) [arXiv:0812.4555];
G. KANE, R. LU AND S. WATSON, arXiv:0906.4765.
- [55] K. CHEUNG, P.Y. TSENG AND T.C. YUAN, *Phys. Lett. B* **678**, 293 (2009) [arXiv:0902.4035].
- [56] I.Z. ROTHSTEIN, T. SCHWETZ AND J. ZUPAN, *J. Cosmol. Astropart. Phys.* **07**, 018 (2009) [arXiv:0903.3116].
- [57] T. SJOSTRAND, S. MRENNNA AND P. SKANDS, *J. High Energy Phys.* **05**, 026 (2006) [hep-ph/0603175].
- [58] J.N. BAHCALL AND R.M. SONEIRA, *Astrophys. J. Suppl.* **44**, 73 (1980).
- [59] J.F. NAVARRO, C.S. FRENK AND S.D. WHITE, *Astrophys. J.* **462**, 563 (1996) [astro-ph/9508025].
- [60] K. ISHIWATA, S. MATSUMOTO AND T. MOROI, *J. High Energy Phys.* **05**, 110 (2009) [arXiv:0903.0242].
- [61] K. GRIEST AND M. KAMIONKOWSKI, *Phys. Rev. Lett.* **64**, 615 (1990);
L. HUI, *Phys. Rev. Lett.* **86**, 3467 (2001).
- [62] F. AHARONIAN *et al.* [H.E.S.S. COLLABORATION], *Astropart. Phys.* **29**, 55 (2008) [arXiv:0711.2369].
- [63] E. BORRIELLO, A. CUOCO AND G. MIELE, arXiv:0903.1852;
M. CIRELLI AND P. PANCI, *Nucl. Phys.* **B821**, 399 (2009) [arXiv:0904.3830];
S. PROFUMO AND T.E. JELTEMA, *J. Cosmol. Astropart. Phys.* **07**, 020 (2009) [arXiv:0906.0001].

- [64] P. SREEKUMAR *et al.* [EGRET COLLABORATION], *Astrophys. J.* **494**, 523 (1998) [astro-ph/9709257];
A. W. STRONG, I. V. MOSKALENKO AND O. REIMER, *Astrophys. J.* **613**, 962 (2004) [astro-ph/0406254].
- [65] J. HISANO *et al.*, *Phys. Rev. D* **79**, 043516 (2009) [arXiv:0812.0219];
J. LIU, P.F. YIN AND S.H. ZHU, *Phys. Rev. D* **79**, 063522 (2009) [arXiv:0812.0964].
- [66] S. TORII *et al.* [PPB-BETS COLLABORATION], arXiv:0809.0760.
- [67] F. AHARONIAN *et al.* [H.E.S.S. COLLABORATION], *Phys. Rev. Lett.* **101**, 261104 (2008) [arXiv:0811.3894];
F. AHARONIAN *et al.* [H.E.S.S. COLLABORATION], arXiv:0905.0105.
- [68] M. CIRELLI, M. KADASTIK, M. RAIDAL AND A. STRUMIA, *Nucl. Phys.* **B813**, 1 (2009) [arXiv:0809.2409];
D. FELDMAN, Z. LIU AND P. NATH, *Phys. Rev. D* **79**, 063509 (2009) [arXiv:0810.5762];
R. ALLAHVERDI *et al.*, *Phys. Rev. D* **79**, 075005 (2009) [arXiv:0812.2196];
I. GOGOLADZE, R. KHALID, Q. SHAFI AND H. YUKSEL, *Phys. Rev. D* **79**, 055019 (2009) [arXiv:0901.0923];
C. BALAZS, N. SAHU AND A. MAZUMDAR, *J. Cosmol. Astropart. Phys.* **07**, 039 (2009) [arXiv:0905.4302];
Y. BAI, M. CARENA AND J. LYKKEN, *Phys. Rev. D* **80**, 055004 (2009) [arXiv:0905.2964];
X.J. BI, R. BRANDENBERGER, P. GONDOLO, T.J. LI, Q. YUAN AND X.M. ZHANG, arXiv:0905.1253;
F. CHEN, J.M. CLINE AND A.R. FREY, arXiv:0907.4746;
D. FELDMAN, Z. LIU, P. NATH AND B.D. NELSON, arXiv:0907.5392.
- [69] A.B. LAHANAS, N.E. MAVROMATOS AND D.V. NANOPOULOS, *Phys. Lett. B* **649**, 83 (2007) [hep-ph/0612152];
M. DREES, H. IMINNIYAZ AND M. KAKIZAKI, *Phys. Rev. D* **76**, 103524 (2007) [arXiv:0704.1590].
- [70] N. OKADA AND O. SETO, *Phys. Rev. D* **70**, 083531 (2004) [hep-ph/0407092];
T. NIHEI, N. OKADA AND O. SETO, *Phys. Rev. D* **71**, 063535 (2005) [hep-ph/0409219].